Non-linear properties of thermal convection

1978 Rep. Prog. Phys. 41 1929

(http://iopscience.iop.org/0034-4885/41/12/003)

Rep. Prog. Phys., Vol. 41, 1978. Printed in Great Britain

Non-linear properties of thermal convection

F H BUSSE

Institute of Geophysics and Planetary Physics, University of California, Los Angeles, California 90024, USA

Abstract

Thermal convection in a layer heated from below is an exemplary case for the study of non-linear fluid dynamics and the transition to turbulence. In this review an outline is given of the present knowledge of the simplest realisation of convection in a layer of fluid satisfying the Oberbeck–Boussinesq approximation. Non-linear properties such as the dependence of the heat transport on Rayleigh and Prandtl numbers and the stability properties of convection rolls are emphasised in the discussion. Whenever possible, theoretical results are compared with experimental observations. A section on convection in rotating systems has been included, but the influence of other additional physical effects such as magnetic fields, side wall geometry, etc, has not been considered.

This review was received in May 1978.

0034–4885/78/0012–1929 $05.00

Contents

1. Introduction

Thermal convection occurs in so many forms in nature and over such a wide range of scales that it could be claimed with some justification that convection represents the most common fluid flow in the Universe. Convection accomplishes the heat transport in stars wherever the radiative transfer is not efficient enough. It warms the Earth's atmosphere by the upward transfer of heat absorbed at the ground. Convective motions are responsible for much of the mixing of water masses occurring in the oceans, and it is widely believed that thermal convection is the basic cause of most tectonic processes in the Earth's crust, including the phenomenon of continental drift. It is also likely that the geomagnetic field is produced by the dynamo action of convection flow in the liquid core of the Earth. Part of the fascination of the subject of convection stems from the fact that the motions in an evaporating puddle of water are described by essentially the same equations as the huge turbulent eddies visible on the surface of the Sun.

But convection is not confined to the natural environment. Wherever heat transfer must be considered in industrial applications thermal convection enters in various forms. In nuclear reactors, in crystallisation processes and in solar heating devices convection plays a crucial role and the rapidly expanding literature on applications of convection indicates a continuing demand for an improved understanding of its properties.

On a more fundamental level thermal convection has received attention as a particularly simple system in which the transition to turbulence can be studied. Experiments on turbulent convection have yielded remarkable and unexpected results which have led to new insights into the nature of turbulent fluid flow. These will be pointed out in various sections of this review. The relative simplicity of convection patterns even in the case of turbulent motion is also one of the reasons for the esthetic attraction of convection. The delightful experience of the visualisation of the spontaneously occurring cellular patterns of convection and their changes in time has always provided a strong and not often recognised motivation for the scientific research.

The field of thermal convection and related flow phenomena has expanded rapidly in the past two decades and even a sizeable monograph could hardly do justice to the large body of scientific results. In this review our attention will be focused on those non-linear properties of convection in a horizontal layer heated from below which seem to have a general importance. No attempt is being made to give a complete review of particular topics. Because the literature on convection probably includes more than a thousand titles even if the numerous papers on applications are not counted, the references listed at the end of the review represent only a tiny and sometimes arbitrarily selected fraction of the published work. For detailed descriptions of linear problems of convection we refer to the books of Chandrasekhar (1961) and Gershuni and Zhukovitskii (1976). Chapters on thermal convection are included in the books by Turner (1973) and Joseph (1976). Reviews of recent research on convection have been given by Spiegel (1971, 1972), Koschmieder (1974), Palm (1975) and Normand *et al* (1977).

2. Basic equations

2.1. *Rayleigh number and Prandtl number*

Since both hydrodynamic and thermal properties of fluids enter into the description of convection, it may be expected that a large number of parameters must be introduced in formulating the basic equations of the problems. Fortunately only two non-dimensional parameters are needed for most applications. To get a feeling for the meaning of the Rayleigh and Prandtl numbers we consider a horizontal fluid layer heated from below and determine the energy requirements for the onset of convection. The energy L_D lost per unit time by viscous dissipation must be supplied by the release L_P of potential energy which is available in systems with a density gradient in the direction opposite to gravity. Using the thickness d of the layer as the typical length scale and V as the typical velocity we obtain:

$$L_D = c_1 \rho_0 \nu V^2/d^2 \tag{2.1}$$

when ν is kinematic viscosity and c_1 is a numerical constant depending on the boundary conditions. Assuming a linear dependence of the density on temperature:

$$\rho = \rho_0[1-\gamma(T-T_0)] \tag{2.2}$$

the maximum available potential energy that can be released is given by $\rho_0\gamma(T_2-T_1)g$, where T_2 and T_1 are the temperatures of the lower and the upper boundaries, respectively, and g is the acceleration due to gravity. But as a fluid particle moves upward or downward its density changes because of thermal conduction. How much a fluid particle is capable of retaining its original density depends on the ratio Vd/κ where κ is the thermal diffusivity. κ/d can be regarded as the typical velocity with which isotherms distorted on a scale d return to their equilibrium position. For small values of V for which expression (2.1) is valid only the fraction Vd/κ of the maximum available potential energy can be released and we obtain for the release per unit time:

$$L_P = c_2 V \rho_0 \gamma (T_2 - T_1) g\, Vd/\kappa \tag{2.3}$$

where c_2 is another numerical constant depending on the boundary conditions. The onset of convection requires $L_P/L_D \geqslant 1$. Since both L_D and L_P are proportional to V^2, the velocity cancels from the ratio and the condition for the instability of the static layer can be written in the form:

$$R \equiv \frac{\gamma(T_2-T_1)gd^3}{\nu\kappa} \geqslant \frac{c_2}{c_1} \equiv R_c. \tag{2.4}$$

R is called the Rayleigh number in honour of Lord Rayleigh who did the first theoretical analysis of the problem in 1916. The numerical value $R_c \equiv c_2/c_1$ is called the critical Rayleigh number. It is typically of the order of 10^3.

The advantage of the choice of the Rayleigh number as basic parameter is that the onset of convection occurs at the same value, R_c, independent of the individual material properties of the convecting fluid. The other basic parameter, the Prandtl number $P = \nu/\kappa$, enters into the theoretical considerations only insofar as the nonlinear properties of convection are concerned. The understanding and determination of the properties of convection as a function of Rayleigh and Prandtl numbers is the main objective of theoretical and experimental research on finite amplitude convection.

2.2. Oberbeck–Boussinesq equations

The fact that the density variations which provide the driving forces of convection are usually relatively small is the basis for the Boussinesq approximation which was first introduced by Oberbeck (1879) in a problem of flow driven by horizontal temperature gradients. In this approximation it is assumed that all material properties are constant with the exception of the temperature dependence of the density (2.2) which is taken into account in the gravity term only. The Oberbeck–Boussinesq approximation implies that the variation of mechanical energy which a fluid particle experiences is small compared to the variation of thermal energy, i.e.:

$$\frac{\gamma\rho_0(T_2-T_1)gd}{c\rho_0(T_2-T_1)}=\frac{\gamma dg}{c}\ll 1 \tag{2.5}$$

where c is the specific heat at constant pressure. In laboratory experiments the inequality (2.5) is very well satisfied since the left-hand side is of the order of 10^{-4}. For geophysical and astrophysical applications the left-hand side becomes of the order of unity when the convection layer extends over a scale height. Even in this case the Oberbeck–Boussinesq equations provide a good approximation if the temperature is interpreted as the 'potential temperature', i.e. if T_2-T_1 is replaced by the excess over the adiabatic temperature difference across the layer. For further details on the Oberbeck–Boussinesq approximation we refer to the papers of Spiegel and Veronis (1960), Mihaljan (1962) and Gray and Giorgini (1976).

Using d, d^2/κ and $(T_2-T_1)/R$ as scales for length, time and temperature, respectively, the Oberbeck–Boussinesq approximation for the equations of motion and the energy equation can be written in the non-dimensional form:

$$P^{-1}\left(\frac{\partial}{\partial t}+\boldsymbol{u}.\boldsymbol{\nabla}\right)\boldsymbol{u}=-\nabla\pi+\theta\boldsymbol{\lambda}+\nabla^2\boldsymbol{u} \tag{2.6(a)}$$

$$\boldsymbol{\nabla}.\boldsymbol{u}=0 \tag{2.6(b)}$$

$$\left(\frac{\partial}{\partial t}+\boldsymbol{u}.\boldsymbol{\nabla}\right)\theta=R\boldsymbol{u}.\boldsymbol{\lambda}+\nabla^2\theta \tag{2.6(c)}$$

where $\boldsymbol{\lambda}$ is the unit vector opposite to the direction of gravity. All terms in the equation of motion (2.6(a)) that can be written in the form of a gradient have been combined in the 'pressure' term, $\nabla\pi$, since only the curl of the equation enters into the analysis of the problem. The energy equation (2.6(c)) has been written in terms of the deviation θ of the temperature from the static distribution. We note that in the limit (2.5) the work done by compression as well as the heat generated by viscous dissipation can be neglected in equation (2.6(c)).

2.3. The linear problem

When the amplitude of convection is small such that the terms $\boldsymbol{u}.\nabla\boldsymbol{u}$ and $\boldsymbol{u}.\boldsymbol{\nabla}\theta$ can be neglected, equations (2.6) become linear homogeneous. Since it has been shown (Chandrasekhar 1961) that the instability of the static layer occurs in the form of monotonically growing disturbances the analysis of convection near the point of marginal stability can be restricted to the time-independent problem. In the older literature this case is described by the expression 'principle of exchange of stabilities'. Assuming a Cartesian system of coordinates with the z coordinate in the vertical

direction, the analysis of the stationary linear problem yields solutions for the z component of the convection velocity of the form:

$$u_z^{(0)} = \left[\sum_n c_n \exp(i\boldsymbol{k}_n.\boldsymbol{r})\right] f(z, \alpha) \tag{2.7}$$

where $\boldsymbol{r}$ denotes the position vector. Because the physical conditions of the convection layer are isotropic with respect to the horizontal directions, the vectors $\boldsymbol{k}_n$ are arbitrary apart from the requirement that they have the same absolute value α:

$$|\boldsymbol{k}_n| = \alpha \qquad \boldsymbol{k}_n.\boldsymbol{\lambda} = 0 \qquad \text{for all } n. \tag{2.8}$$

The function $f(z, \alpha)$ is determined by an ordinary differential equation depending on α as parameter. Two different kinds of boundary conditions are usually considered. The assumption of stress-free boundaries is very popular because it leads to a simple solution for $f(z, \alpha)$:

$$u_z = \frac{\partial^2}{\partial z^2} u_z = \theta = 0 \qquad \text{at} \qquad z = \pm \tfrac{1}{2}. \tag{2.9}$$

The vanishing of the second derivative of u_z is a consequence of the continuity equation (2.6(b)) and the fact that $\partial u_x/\partial z$ and $\partial u_y/\partial z$ vanish at the boundary. For stress-free boundaries $f(z, \alpha)$ becomes actually independent of α:

$$f(z, \alpha) = \sqrt{2} \cos \pi z \qquad R(\alpha) = (\pi^2 + \alpha^2)^3/\alpha^2. \tag{2.10}$$

The minimum value R_c of the function $R(\alpha)$ represents the critical value of the Rayleigh number at which convection first sets in when the temperature difference across the layer is slowly increased:

$$R_c = 27\,\pi^4/4 \qquad \alpha_c = \pi/\sqrt{2}. \tag{2.11}$$

The property that convection with $\alpha > \alpha_c$ requires a higher Rayleigh number is mainly a consequence of the increased heat conduction between up- and down-going fluid parcels which diminishes the release of potential energy. On the other hand, convection with a large wavelength is not favoured because the work done by the vertical motion becomes too small in comparison to the energy consumed by the viscous dissipation of the horizontal motion.

In the case of the more realistic rigid boundary conditions:

$$u_z = \frac{\partial}{\partial z} u_z = \theta = 0 \qquad \text{at} \qquad z = \pm \tfrac{1}{2} \tag{2.12}$$

numerical computations (Pellew and Southwell 1940, Reid and Harris 1958) have yielded:

$$R_c = 1707{\cdot}76 \qquad \alpha_c = 3{\cdot}117.$$

The increase of the Rayleigh number R_c in comparison with the result (2.11) indicates the constraining effect of the rigid boundaries on the horizontal motions.

3. Weakly non-linear convection

3.1. The perturbation approach

The manifold of eigensolutions of the form (2.7) exhibits a two-fold degeneracy. First, there is the orientational degeneracy associated with the unrestrained choice

of the directions of the vectors $\boldsymbol{k}_n$. The second degeneracy corresponds to the infinite variety of circulation patterns that are realised for different values of the coefficients c_n. These coefficients are arbitrary complex numbers, subject only to the normalisation condition:

$$\sum_{n=-N}^{N} |c_n|^2 = 1 \tag{3.1}$$

and the conditions:

$$c_{-n} = c_n^+ \qquad n = 1, \ldots, N$$

where c_n^+ denotes the complex conjugate of c_n, and where the assumption has been made that N different $\boldsymbol{k}$ vectors contribute in expression (2.7) with $\boldsymbol{k}_{-n} = -\boldsymbol{k}_n$.

The orientational degeneracy cannot be removed since the fact that no horizontal direction is distinguished is an intrinsic property of the problem, but the pattern degeneracy can be removed to a large extent by considering the non-linear problem. As a result, only a small fraction of the manifold (2.7) of the solutions of the linear problem corresponds to possible solutions of the non-linear problem in the limit of vanishing amplitude of convection.

The perturbation approach to the non-linear problem posed by equations (2.6) is based on an expansion in powers of the amplitude ϵ of convection:

$$u_z = \epsilon(u_z^{(0)} + \epsilon u_z^{(1)} + \epsilon^2 u_z^{(2)} + \ldots) \tag{3.2(a)}$$

$$R = R_c + \epsilon R^{(1)} + \epsilon^2 R^{(2)} + \ldots . \tag{3.2(b)}$$

Power series analogous to (3.2(a)) are assumed for the other dependent variables. Obviously, the expansion (3.2) is not a suitable approach to derive quantitative information about convection beyond the immediate neighbourhood of the critical Rayleigh number. But it still represents the only way to analyse the variety of three-dimensional solutions of equations (2.6). The perturbation approach (3.2) was introduced independently by Gorkov (1957) and Malkus and Veronis (1958). A systematic analysis of the manifold of solutions (2.7) and an investigation of the stability properties has been given by Schlüter *et al* (1965). Kuo (1961) used a slightly different perturbation parameter instead of ϵ and was able to obtain a good approximation for the two-dimensional solution for Rayleigh numbers up to $10R_c$. The perturbation method has been applied to a variety of other convection problems, for example to the case of a rotating layer discussed in §7.2.

In the case of equations (2.6) the solvability conditions require $R^{(n)} = 0$ for odd integers n when the boundary conditions are symmetric. This is a consequence of the symmetry of the non-linear advection terms in the equations. Even when different conditions are applied at the lower and the upper boundaries $R^{(1)} = 0$ still holds in general. To obtain a non-trivial result, equations (2.6) must be considered in the order ϵ^3. Since the operator described by the linear part of equations (2.6) and boundary conditions (2.9) or (2.12) is self-adjoint, the solvability conditions require that the inhomogeneities are orthogonal to arbitrary solutions of the homogeneous problem. In the order ϵ^3 a set of $2N$ equations of the form:

$$0 = \sum_{n=-N}^{N} A(\boldsymbol{k}_e . \boldsymbol{k}_n) c_n c_{-n} c_e - R^{(2)} c_e \qquad \text{for} \qquad e = -N, \ldots, -1, +1, \ldots, N \tag{3.3}$$

is obtained. Together with condition (3.1) the system of $2N+1$ non-linear equations determines the $2N+1$ unknowns $c_{-N}, \ldots, c_N, R^{(2)}$. Because the function A depends

only on the angle between the vectors $\boldsymbol{k}_e$ and $\boldsymbol{k}_n$, it is readily seen that the solution:

$$|c_1|^2 = \ldots = |c_N|^2 = 1/2N \tag{3.4}$$

satisfies equations (3.3) if a regular distribution of vectors $\boldsymbol{k}_n$ is prescribed, i.e. if the angle between neighbouring vectors $\boldsymbol{k}_n$ and $\boldsymbol{k}_e$ is always the same (see, for example, figure 1(*a*)). Since only the cosine of the angle enters into equations (3.3), solution (3.4) remains valid in the case of semiregular distributions, i.e. those corresponding to the superposition of two equal regular distributions (figure 1(*b*)). The solutions of physical interest, as for example the two-dimensional solution corresponding to $N=1$ and the hexagonal solution corresponding to $N=3$, are generally represented by regular distributions of $\boldsymbol{k}$ vectors.

The full content of equations (3.3) has not yet been explored, but by imposing additional periodicity requirements the implications of the degenerate bifurcation problem can be analysed in a mathematically rigorous way. For a more detailed

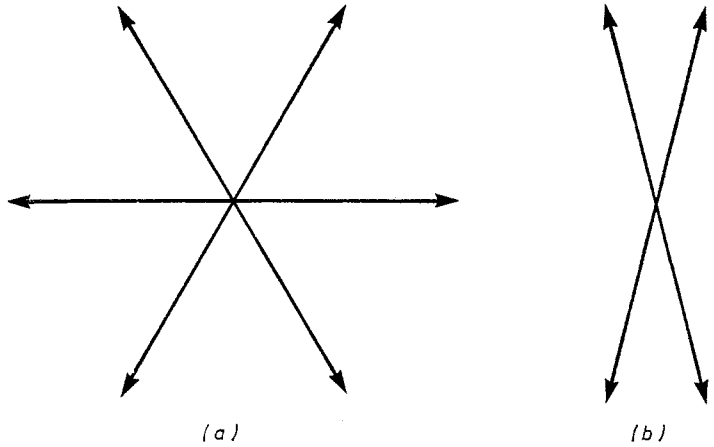

Figure 1. (*a*) Example of a regular distribution of $\boldsymbol{k}$ vectors (hexagon case). (*b*) Example of a semiregular distribution.

discussion of the interesting mathematical aspects of the problem we refer to the chapter on cellular convection in Joseph's (1976) book and to the recent article by Kirchgässner (1977).

3.2. Stability theory

Although the manifold of possible steady solutions of the form (2.7) is strongly restricted by conditions (3.3), the number of solutions of equations (2.6) is still infinite and an additional selection principle is required to distinguish the physically preferred form of convection. The stability with respect to arbitrary disturbances of infinitesimal amplitude provides the suitable selection principle even though it does not guarantee a unique solution. Because of the assumption of infinitesimal amplitude the disturbances satisfy linear homogeneous equations. Without losing generality, an exponential dependence on time, $\exp(\sigma t)$, can be assumed. Thus the equations for the disturbances $\tilde{\boldsymbol{u}}$, $\tilde{\pi}$, $\tilde{\theta}$ of the steady solution $\boldsymbol{u}$, π, θ can be written in the form:

$$P^{-1}(\sigma\tilde{\boldsymbol{u}}+\boldsymbol{u}.\nabla\tilde{\boldsymbol{u}}+\tilde{\boldsymbol{u}}.\nabla\boldsymbol{u})=-\nabla\tilde{\pi}+\tilde{\theta}\boldsymbol{\lambda}+\nabla^2\tilde{\boldsymbol{u}} \tag{3.5(a)}$$

$$\nabla.\tilde{\boldsymbol{u}}=0 \tag{3.5(b)}$$

$$\sigma\tilde{\theta}+\boldsymbol{u}.\nabla\tilde{\theta}+\tilde{\boldsymbol{u}}.\nabla\theta=R\tilde{\boldsymbol{u}}.\boldsymbol{\lambda}+\nabla^2\tilde{\theta}. \tag{3.5(c)}$$

When the series representation (3.2) for the steady solution is introduced in the equations, the appearance of terms proportional to different powers of ϵ suggests a solution of the form:

$$\tilde{u}_z=\tilde{u}_z^{(0)}+\epsilon\tilde{u}_z^{(1)}+\epsilon^2\tilde{u}_z^{(2)}+\ldots \tag{3.6(a)}$$

$$\sigma=\sigma^{(0)}+\epsilon\sigma^{(1)}+\epsilon^2\sigma^{(2)}+\ldots \tag{3.6(b)}$$

and analogous expansions for the other disturbance variables. The analysis of the problem proceeds in close correspondence to the steady problem. In zeroth order the solution for $\tilde{u}_z^{(0)}$ can be written in the form (2.7) with $\tilde{c}_n$ in place of c_n. Even the function $f(\varkappa, \alpha)$ remains the same as in the steady case if the attention is restricted to disturbances with $\sigma_0=0$ which are the most critical ones in the case $\alpha=\alpha_c$. In first order it is found that $\sigma^{(1)}$ vanishes just as $R^{(1)}$ did. The solvability condition in second order yields:

$$-\sigma^{(2)}M\tilde{c}_e=\sum_{n=-N}^{N}A(\boldsymbol{k}_e.\boldsymbol{k}_n)(c_nc_{-n}\tilde{c}_e+\tilde{c}_nc_{-n}c_e+c_n\tilde{c}_{-n}c_e)-R^{(2)}\tilde{c}_e$$
$$\text{for}\qquad e=-N,\ldots,-1,+1,\ldots N \tag{3.7}$$

where M is a positive constant. In addition to these $2N$ equations there are an infinite number of equations arising in the case where a vector $\boldsymbol{k}_e$ of the disturbance solution does not appear among the N $\boldsymbol{k}$ vectors describing the steady solution. But the latter do not yield positive values of $\sigma^{(2)}$, in general, and thus do not require special consideration.

The main question about the system of equations (3.7) is whether eigenvalues $\sigma^{(2)}$ with positive real parts exist, implying instability of the steady solution. This question can be answered in the affirmative for $N\geqslant 2$ without specific knowledge about the steady solution. Using some general properties of the function $A(\boldsymbol{k}_e.\boldsymbol{k}_n)$ Schlüter *et al* (1965) have shown that all eigenvalues $\sigma^{(2)}$ are real and that at least one of them is positive if $N\geqslant 2$. In the case $N=1$, corresponding to convection in the form of two-dimensional rolls, the highest eigenvalue is $\sigma^{(2)}=0$ corresponding to the disturbance given by:

$$\tilde{u}_z^{(0)}\equiv\boldsymbol{k}_1.\nabla u_z^{(0)}. \tag{3.8}$$

It is not surprising that a neutral disturbance of this form exists which describes an infinitesimal translation of the steady solution. Since the influence of lateral boundaries is neglected in the limit of an infinitely extended convection layer an arbitrary horizontal translation of a solution yields another solution. While the neutral disturbance (3.8) does not lead to instability, slightly modified disturbances can sometimes induce instability as discussed in §6.

3.3. Non-symmetric convection layers

The case $N=1$ distinguished by its stability property corresponds to a single solution describing convection in the form of rolls. Although only the absolute value $|c_1|$ is determined by condition (3.4), the multiplication of c_1 by an arbitrary phase factor $\exp(i\phi)$ describes a horizontal translation of the convection pattern (figure 2(*a*)). It can be shown that this property persists in the case $N=2$. All solutions in this case

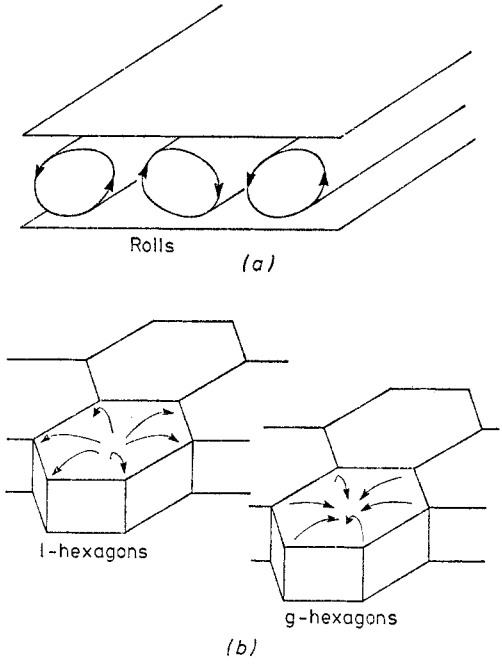

Figure 2. (*a*) Two-dimensional convection in the form of rolls. (*b*) l- and g-type hexagonal convection cells.

represent translations of a single form of convection. But in the case $N=3$ conditions (3.4) do not preclude the existence of several physically different forms of convection which cannot be transformed into each other by a translation.

Since the change of sign of c_1 is equivalent to the change of sign of ϵ in the case $N=1$, it can be concluded that the coefficients $R^{(n)}$ vanish for all odd integers n, even when the symmetry of equations (2.6) is destroyed as, for instance, in the case of temperature-dependent material properties. In the case $N=3$, a change of sign of the coefficients c_n leads to a physically different solution and finite values of $R^{(n)}$ must, in general, be expected for odd integers n when the properties of the convection layer are not symmetric about its midplane. This is the origin of the phenomenon that experiments sometimes exhibit convection rolls and at other times convection in the form of hexagonal cells.

The simplest way to examine the influence of an asymmetric property is to consider the temperature dependence:

$$\rho=\rho_0[1-\gamma(T-T_0)+\beta(T-T_0)^2] \tag{3.9}$$

in place of expression (2.2) for the density, but leave the Oberbeck–Boussinesq approximation intact in all other respects. As a result, non-vanishing values of $R^{(1)}$ and $\sigma^{(1)}$ become possible whenever the condition:

$$\boldsymbol{k}_e+\boldsymbol{k}_n+\boldsymbol{k}_m=0 \tag{3.10}$$

can be satisfied. The simplest solution for which relationship (3.10) holds is the hexagon solution corresponding to $N=3$ in equations (3.4). The two possibilities $c_i=6^{-1/2}$ and $c_i=-6^{1/2}$, $|i|=1, 2, 3$, must be distinguished. We shall refer to the former as the l-hexagon solution, since it is often realised in liquids. The latter

solution is mostly realised in gases and is called the g-hexagon solution for that reason (figure 2(*b*)). Besides those two solutions, there exist two other choices, $c_i = \pm i6^{-1/2}$, which cannot be generated by translations of the hexagon solutions. But those choices are eliminated by the solvability conditions in which the effect of asymmetries has been included.

The general stability analysis outlined in the preceding section can be extended to include the effects of a finite value β as well as the analogous effects of the temperature dependence of other material properties (Busse 1962, 1967a). Restricting the attention to β as the representative parameter, it is found that the roll solution may be displaced by either one of the hexagon solutions as the physically realisable form of convection as shown in figures 3 and 4. It is noteworthy that there is always a region where both solutions are stable. The preference for the hexagon solution in a non-symmetric layer is physically understandable because of the adjustment property. Depending on the sign of the asymmetry, either the l-hexagons or the g-hexagons are optimally

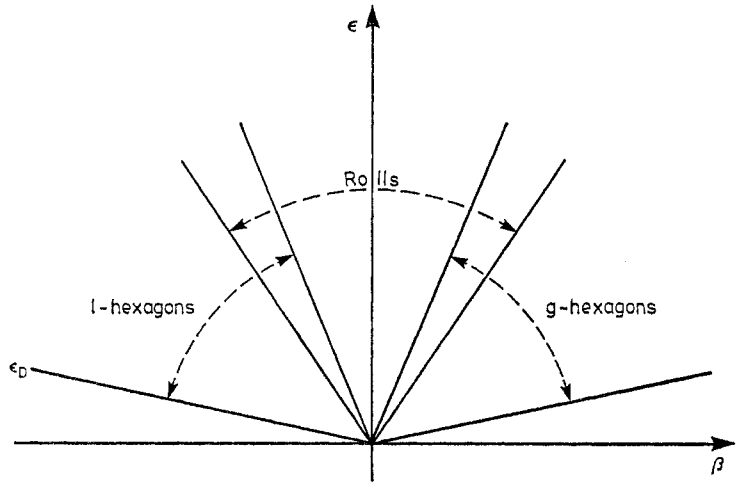

Figure 3. Stability range of convection in the form of rolls and hexagons as a function of the amplitude ϵ and the asymmetry parameter β.

adjusted. The hexagon solution is the simplest solution with this property and the conclusion to be drawn from the stability analysis is that the simplest realisation among solutions with certain properties appears to be preferred.

The temperature dependence of the viscosity is usually the dominant cause of asymmetry in convection layers and its importance for the preference of the hexagon solutions was recognised by Graham (1933) and theoretically supported by Palm (1960) and Segel and Stuart (1962) before the systematic stability analysis was undertaken. The adjustment is such that the viscosity is minimised in the highly strained region in the centre of the convection cell. Thus in liquids, where the viscosity is lower at the bottom, hexagons with upward motion in the centre occur while in gases, for which the viscosity increases with temperature, convection cells show downward motion in the centre. A striking demonstration of this effect has been given by Tippelskirch (1956), who did experiments with liquid sulphur which exhibits both an increasing and a decreasing dependence of the viscosity on temperature.

It is of interest to note that hexagonal cells with rising motion in the centre tend

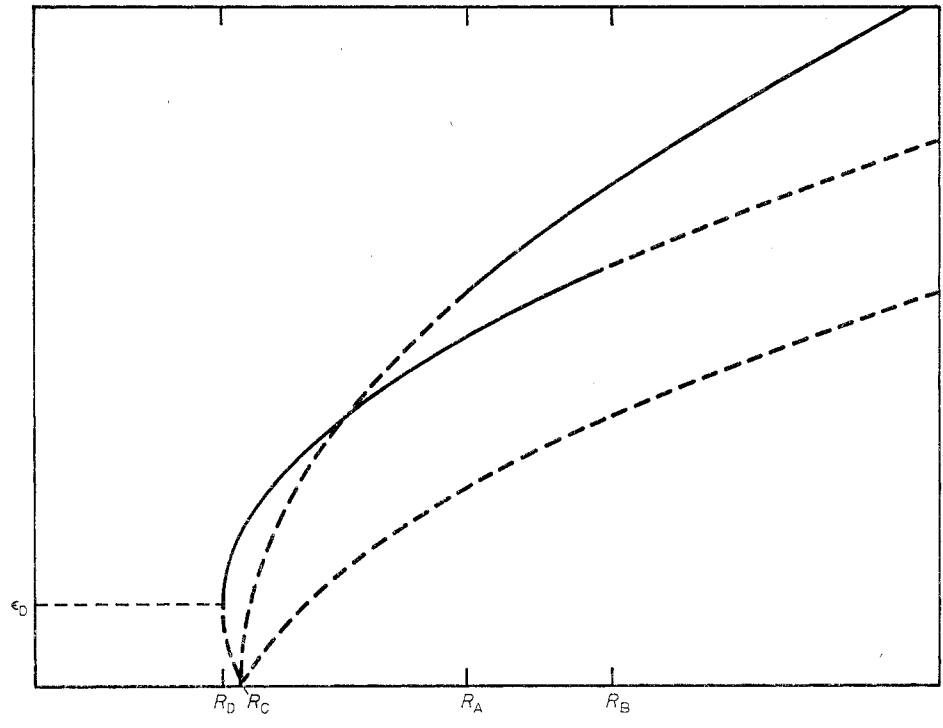

Figure 4. The dependence of the amplitude ϵ of convection on the Rayleigh number for different forms of convection. The respective flows are unstable along the broken parts of the curves. The Rayleigh numbers R_A, R_B, R_D indicate the boundaries of the stability regions.

to be preferred when the layer is contained between a rigid lower boundary and a stress-free upper surface (Busse 1962). This kind of asymmetry does not enter into the expression for $R^{(1)}$, but into the expression for $R^{(3)}$ instead. Thus a quantitative assessment of this case is difficult since contributions of higher order are not negligible. If, on the other hand, the effects of surface tension are taken into account, a non-vanishing contribution to $R^{(1)}$ arises (Davis and Segel 1968), leading again to a preference for hexagonal convection cells which can be evaluated accurately in the limit of small ϵ.

The fact that, for amplitudes less than ϵ_D (see figure 4) all steady solutions are unstable, has the consequence that there exists a regime where no steady state is realisable when the heat flux is the prescribed parameter of the problem instead of the Rayleigh number. It can be shown (Busse 1967c) that the amplitude of hexagonal convection executes non-linear relaxation oscillations in this case.

3.4. An extremum principle

The solvability equations (3.3) and the stability problem (3.7) are equivalent to the conditions that the function:

$$F(C_{-N}, \ldots, C_N) \equiv \tfrac{1}{2}(R-R_c)\sum_n |C_n|^2 + \tfrac{1}{4}\sum_{e,n} A(\boldsymbol{k}_e.\boldsymbol{k}_n)|C_n|^2|C_e|^2 + \tfrac{1}{3}\sum_{e,m,n} \beta_{emn} C_e C_m C_n \quad (3.11)$$

assumes a maximum in the case of the stable solution. In expression (3.11) the definitions:

$$C_n \equiv \epsilon c_n$$

$$\beta_{emn} \equiv \begin{cases} \beta B & \text{for } \boldsymbol{k}_e + \boldsymbol{k}_m + \boldsymbol{k}_n = 0 \\ 0 & \text{otherwise} \end{cases}$$

have been used where B is a constant. The dependence of the function (3.11) on the coefficient β has been included in order to demonstrate the way in which small asymmetries of the convection layer enter into the stability analysis. All summations in expression (3.11) run from $-N$ to $+N$, with the exception of 0.

The necessary conditions for a stationary value of F as a function of the variables C_n is the vanishing of the first derivatives:

$$0 = \frac{\partial F}{\partial C_n} = (R - R_c) C_n^+ + \sum_e A(\boldsymbol{k}_e . \boldsymbol{k}_n) |C_e|^2 C_n^+ + \sum_{e,m} \beta_{emn} C_e C_m$$

$$\text{for} \qquad n = -N, \ldots, N. \qquad (3.12)$$

These equations represent the solvability equations for small-amplitude solutions of the form (2.7). Obviously equations (3.12) are identical to equations (3.3) in the limit $\beta = 0$ except for a factor of $-\epsilon^2$.

A sufficient condition for a maximum of F is that the matrix of the second derivatives of F is negative definite. This condition is equivalent to the condition that all eigenvalues $\sigma = \epsilon\sigma^{(1)} + \epsilon^2\sigma^{(2)}$ are negative definite. In the case $\beta = 0$, this equivalence follows from the fact that the matrix of the coefficients of the unknown $\tilde{c}_e$ on the right-hand side of equations (3.7) is identical to the matrix of the second derivatives of F divided by $-\epsilon^2$. For further details see Busse (1967a).

A physical interpretation of the extremum principle can be obtained by using the property that the dimensionless convective heat transport H is given by $g\epsilon^2 \equiv g\Sigma_n |C_n|^2$ where g is a constant. Expression (3.11) can be written in the form:

$$F = \hat{H}(R - R_0)/2g - \int_0^{\hat{H}} (\hat{R}(H') - R_c)\, dH'/2g \qquad (3.13)$$

where

$$R(\hat{H}) \equiv R_c - \epsilon^2 \sum_{e,n} A(\boldsymbol{k}_e . \boldsymbol{k}_n) |c_n|^2 |c_e|^2 + \epsilon \sum_{e,m,n} \beta_{emn} c_e c_m c_n$$

is a general definition of the Rayleigh number for all solutions of the form (2.7) including those which do not satisfy the solvability conditions. A consequence of the property that expression (3.13) assumes a maximum for the stable solution is that the upper branch of the two solutions existing for $R_D \leqslant R < R_c$ (see figure 4) is stable while the lower branch is unstable because it corresponds to a lower value of F at a given value of R. In the special case $\beta = 0$:

$$F = \hat{H}(R - R_c)/4g \qquad (3.14)$$

and thus a maximum of F corresponds to a maximum of the heat transport at a given value of R. The hypothesis that the realised form of convection tends to maximise the heat transport has been used by Malkus (1954a) and Malkus and Veronis (1958). In general, this hypothesis is not true, but in the particular limit $R \to R_c$, $\beta = 0$, it turns out to be a special case of the extremum principle. The fact that the hypothesis does not hold for $\beta \neq 0$ is evident from figure 4. The roll solution remains unstable even where it exceeds the heat transport of the stable hexagon solution. Since the maximum

principle describes a local property, it does not exclude the possibility that both rolls and hexagons are stable solutions. Indeed, the Rayleigh number for which expression (3.13) becomes equal for rolls and hexagons lies between R_A and R_B.

Because it is valid only for terms of second order in ϵ, the extremum principle has limited value. It can be applied to other stability problems exhibiting isotropy with respect to two dimensions as long as the matrix of the coefficients of the disturbance amplitudes $\tilde{c}_e$ remains symmetric. In the case of a convection layer rotating about a vertical axis, this property is lost because the function A depends on $(\boldsymbol{k}_e \times \boldsymbol{k}_m).\boldsymbol{\lambda}$ as well as on $\boldsymbol{k}_e.\boldsymbol{k}_m$. For a somewhat different interpretation of the extremum principle restricted to the case $\beta = 0$, see Palm (1972).

4. Observational evidence

4.1. The onset of convection

The results of the weakly non-linear theory of convection are basically confirmed by laboratory observations. Within the experimental accuracy the onset of convection occurs at the critical value of the Rayleigh number predicted by linear theory. When the deviations from the Oberbeck–Boussinesq approximation are small, the convection flow assumes the form of nearly two-dimensional rolls, but in the intermediate neighbourhood of the critical Rayleigh number hexagonal cells are often observed. The transition from hexagonal convection to roll convection is well exhibited in the photographs of Silveston (1958) and Somerscales and Dougherty (1970). A detailed quantitative comparison between theory and experimental data is difficult because the theoretical assumption of an infinite layer is not well approximated in most experimental apparatus. The side walls influence the formation of the convection pattern significantly if the aspect ratio between the width L and the depth d of the layer is of the order of 30 or less. Thus convection rolls assume the form of ring cells in Koschmieder's (1966) experiments with a circular layer. In Krishnamurti's (1968) experiments, the rolls tend to align themselves with the side walls of the rectangular layer.

Even in the case of much larger aspect ratios than those commonly used in laboratory experiments, it is conceivable that the side walls ultimately play a role in determining the convection pattern. As convective motions grow from random initial conditions, patches of rolls tend to form with varying orientation of the rolls. At the boundaries between the patches, adjustment processes take place in which some patches grow at the expense of others. The typical time scale for these time-dependent processes is l^2/κ where l is a typical diameter of the patches. Thus an asymptotic steady state is approached on a relatively large time scale which ultimately becomes L^2/κ, at which point the influence of the side walls will be noticeable. The interesting statistical problem associated with the double limit $L \to \infty$, $t \to \infty$ has not yet been investigated. Some experimental data on the time dependence as a function of the aspect ratio have recently been obtained by Ahlers and Behringer (1978).

The development of laser Doppler shift velocity meters has allowed measurement of the convective motion in detail. Berge (1975) reports experimental results of this kind and finds good agreement with the predictions of the weakly non-linear theory. Convection in a layer heated from below is one of the few cases of hydrodynamic instability for which detailed quantitative agreement between experiment and theory has been obtained. The comparison shows little influence of imperfections, which play a dominant role in the occurrence of shear flow instabilities, and in the case of the

buckling instability of elastic shells and rods (Reiss 1977, Stuart 1977). More recently, the measurements of the spatial structures of the convection flow have been extended to higher Rayleigh number (Dubois and Berge 1978) in order to compare the Fourier analysis of the data with the theoretically computed amplitudes of the higher harmonics of the velocity field. Again, good agreement is found.

4.2. The convective heat transport

The determination of the heat transport as a function of the Rayleigh number is traditionally regarded as the most important problem of research on convection, and many of the early experiments have been devoted exclusively to this task. In the non-dimensional formulation of equations (2.6) the average heat transport H is given by:

$$H = R + \langle \boldsymbol{u} . \boldsymbol{\lambda} \theta \rangle$$

where the brackets $\langle \ldots \rangle$ denote the average over the convection layer. To obtain a measure of the efficiency of convection, the Nusselt number Nu has been introduced, which is defined as the ratio between the heat transport both with and without convection:

$$Nu = H/R = 1 + \langle \boldsymbol{u} . \boldsymbol{\lambda} \theta \rangle / R. \tag{4.1}$$

It is convenient to represent the data obtained at high Rayleigh numbers in the form of a power law. Even though power laws seem to fit the measurements over an extensive range of Rayleigh numbers, it is doubtful whether asymptotic relationships can be obtained from laboratory experiments which rarely exceed a Rayleigh number of the order of 10^{10}. Mixing length theory (Kraichnan 1962) suggests that the power law relationship for the Nusselt number may change at Rayleigh numbers as high as 10^{24}. The experimental measurements exhibit a relatively small but significant dependence on the Prandtl number. The power law relationships:

$$Nu = 0{\cdot}184\, R^{0{\cdot}281} \qquad \text{for } P = 200 \tag{4.2(a)}$$

$$Nu = 0{\cdot}183\, R^{0{\cdot}278} \qquad \text{for } P \approx 7 \tag{4.2(b)}$$

$$Nu = 0{\cdot}123\, R^{0{\cdot}294} \qquad \text{for } P = 0{\cdot}7 \tag{4.2(c)}$$

$$Nu = 0{\cdot}147\, R^{0{\cdot}247} \qquad \text{for } P = 0{\cdot}025 \tag{4.2(d)}$$

represent the measurements of Rossby (1969), Chu and Goldstein (1973), Goldstein and Chu (1971) and Rossby (1969), respectively. The results (4.2(a)) and (4.2(b)) are identical within the experimental accuracy, but the relationship (4.2(c)) obtained for air shows a distinctly steeper increase of the heat transport with Rayleigh number. This result agrees with the relationship $Nu = 0{\cdot}13\, R^{0{\cdot}30}$ of Fitzjarrald (1976), whose experiment on convection in air included data for $R = 10^{10}$.

When accurately measured and closely spaced values of the heat transport are plotted as a function of R, the onset of convection is clearly noticeable by the change in the slope of the curve. More surprising is the property that additional kinks appear at higher Rayleigh numbers. Schmidt and Saunders (1938) reported a kink at $R \sim 5 \times 10^4$. When Malkus (1954a) did experiments with a slowly decaying Rayleigh number he counted a total of six supercritical kinks, the highest occurring at a value of R of the order of 10^7. Because convection is highly turbulent at those high Rayleigh numbers, the evidence for discrete transitions contradicts the idea that turbulent fluid systems are governed by smoothly varying statistical properties. Indeed, the dis-

covery of the transitions has stimulated some new theoretical approaches to the problem of turbulence which suggest that the existence of discrete structure in turbulent fluid systems is the rule rather than the exception. The Malkus transitions have been confirmed by numerous investigators (Willis and Deardorff 1967, Carroll 1971, Chu and Goldstein 1973, Threlfall 1975). While there seems to be general agreement about the transitions at $R=2\times10^4$ and $R=6\times10^4$, some others appear at different values of R in different experiments. Those shifts may be due to variations of the Prandtl number or even the aspect ratio of the convection layer (Threlfall 1975). The identification of the kinks with changes in the pattern of convection has been only partially successful. The transition at $R\sim2\times10^4$ clearly corresponds to the onset of bimodal convection (Krishnamurti 1970a, Busse and Whitehead 1971) and the transition at $R\sim6\times10^4$ seems to be related to the onset of time dependence in the case of fluids with moderately high Prandtl number. More detailed observations on the Prandtl number dependence of the transitions are desirable.

4.3. Observations of transitions

While the exact location and the reproducibility of the higher kinks of the heat transport curve have remained a somewhat controversial subject, a more definitive picture has emerged for those transitions of convection which can be observed directly. Detailed visual observations and simultaneous heat transport measurements have been carried out by Krishnamurti (1970a, b, 1973). Figure 5 shows a slightly modified version of the transition diagram which Krishnamurti used in order to present her data and those of other investigators in a comprehensive fashion.

In moderate and high Prandtl number fluids, steady two-dimensional rolls represent the physically realised form of convection up to $R\sim2\times10^4$. At that point a transition to steady three-dimensional convection is observed. Since this form of convection seems to consist of two roll patterns superimposed at a right angle, it has been called bimodal convection. The third transition leading to time-dependent three-dimensional convection flow is less clearly defined because it appears to depend on inhomogeneities of the convection pattern. Krishnamurti (1970b) reports on onset of oscillations at a Rayleigh number of about 6×10^4, independent of P if P is sufficiently large. Busse and Whitehead (1974) found that the onset of oscillations occurred at a Rayleigh number increasing linearly with P if a homogeneous pattern of bimodal convection had been established. But they also found isolated spots of oscillating convection at much lower Rayleigh numbers when the pattern of convection was inhomogeneous. Whitehead and Parsons (1978) investigated high Prandtl number convection in considerable detail and found that oscillations did not occur below a Rayleigh number which increases slightly with P. On the basis of these results, the high Prandtl number regime of figure 5 has been drawn.

At low Prandtl number the onset of oscillations precedes the transition from rolls to steady three-dimensional convection. The instability assumes the form of a wavy transverse shift of the convection roll which propagates along the axis of the roll pattern as indicated schematically in figure 6. Observations of the oscillations in air by Willis and Deardorff (1970) show clearly the sinusoidal nature of the waves as long as their amplitude remains sufficiently small. As the amplitude of the oscillations increases the time dependence appears to become aperiodic and a broad spectrum replaces the discrete peaks corresponding to the frequency of oscillation and its higher harmonics. The exact way in which the transition to aperiodic time dependence

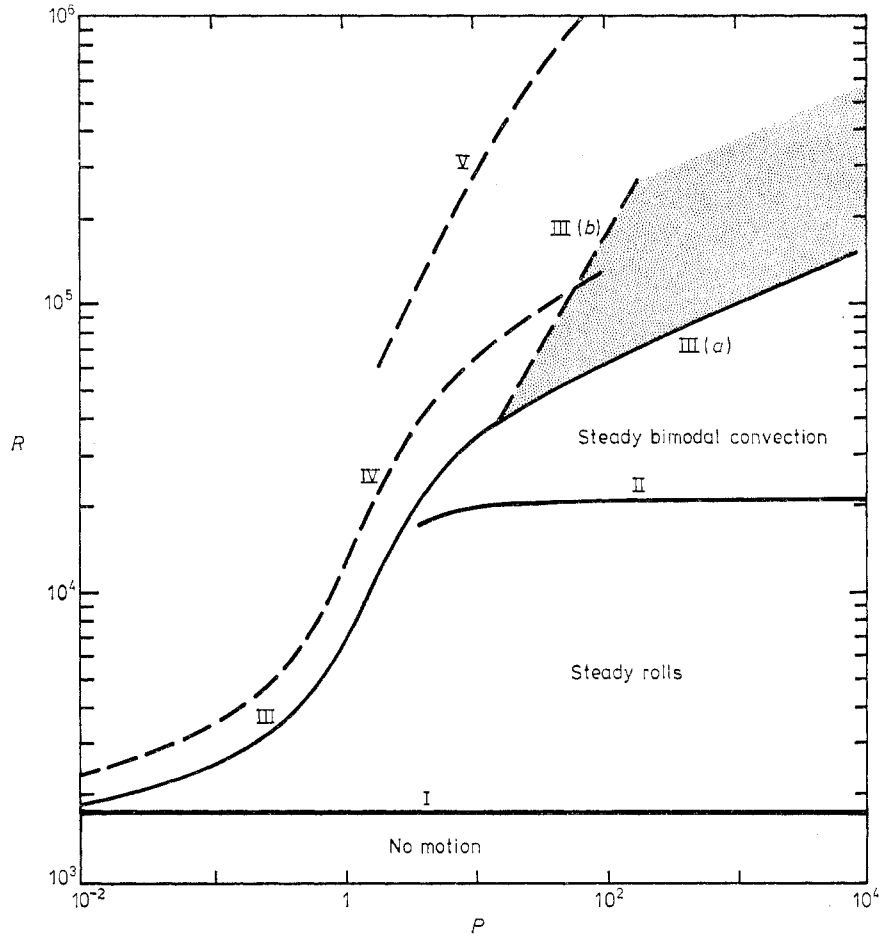

Figure 5. Transitions in convection as a function of Rayleigh and Prandtl numbers after Krishnamurti (1973) and others. The curves indicate the onset of steady rolls (I), three-dimensional convection pattern (II), time-dependent convection (III) in isolated spots (III(*a*)) and uniformly throughout the layer (III(*b*)), and turbulent convection (IV).

occurs is obviously important to the problem of the onset of turbulence and thus has become a subject of intense research (Gollup *et al* 1977).

At moderate Prandtl numbers, turbulent convection at Rayleigh numbers of the order of 10^5–10^7 exhibits the typical structure of relatively steady large-scale cells in which highly fluctuating (both in space and in time) small-scale convection elements are imbedded. Because these elements seem to be oriented predominantly towards the centre of the cells, they resemble spokes and this form of convection has been called spoke pattern convection (Busse and Whitehead 1974). Little is known about this form of convection which seems to combine random processes with the permanence of a large-scale organising structure. Because of the complexity of spoke pattern convection it is not surprising that no visual observations of further transitions do exist. New experimental techniques are required to clarify the role of discrete transitions in turbulent convection. The optical correlation method of Somerscales and Parsapour (1976) may provide a useful instrument for research in this direction.

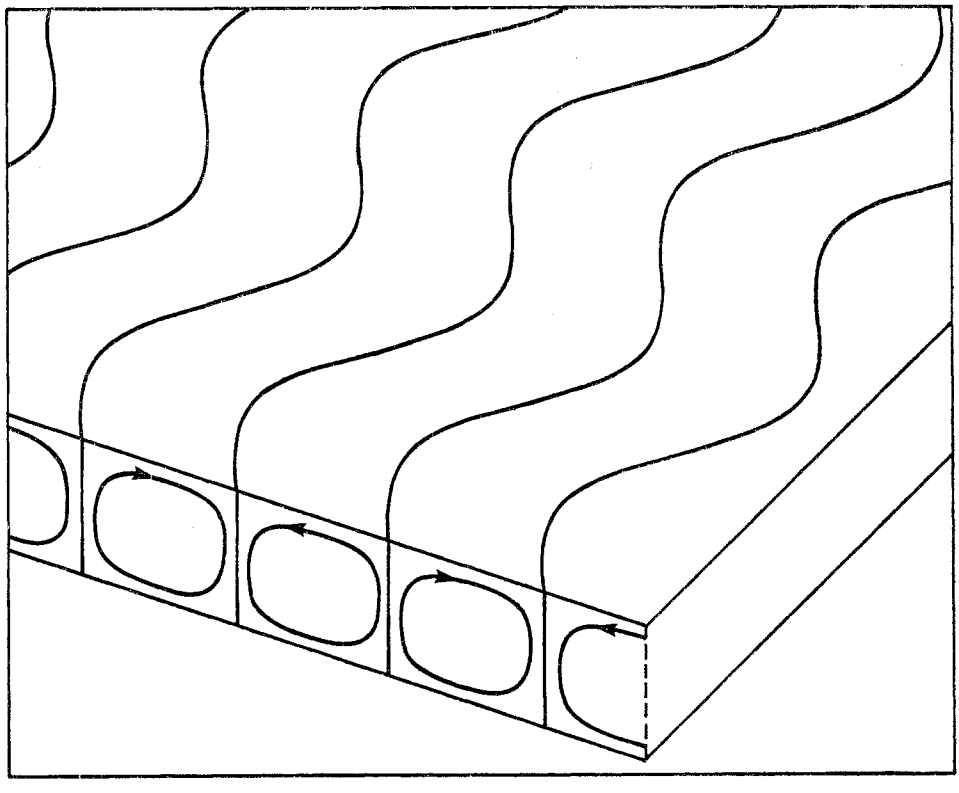

Figure 6. Qualitative sketch of oscillatory convection (from Clever and Busse 1974). The waves propagate along the convection rolls.

5. The strongly non-linear problem

5.1. Numerical computations

The property that convection rolls are physically preferred according to the small-amplitude stability theory, combined with the well-behaved nature of the mathematical problem, has made the problem of two-dimensional convection a favoured subject of numerical analysis ever since the first sufficiently fast computers became available in the early sixties. New numerical methods have been developed in the context of the convection problem (see, for example, Chorin 1967) and the efficiency of older methods has been improved by a large number of investigators. Both finite difference methods and Galerkin procedures have yielded good results with the larger flexibility of the former balanced by the fact that the latter can be easily combined with a stability analysis, as will be discussed in §6.

Finite difference solutions were first obtained by Deardorff (1964) and Fromm (1965) for stress-free as well as rigid boundaries, while Galerkin solutions were produced by Veronis (1966), in the case of free boundaries, and by Busse (1967b), in the case of rigid boundaries. Since then, the parameter range of the computations has been vastly extended by the work of Schneck and Veronis (1967), Plows (1971), Moore and Weiss (1973) and others. The most interesting result of the computations is the dependence of the Nusselt number on the Rayleigh number. For stress-free

boundaries, Moore and Weiss (1973) find:

$$Nu = 1{\cdot}8\,(R/R_c)^{0{\cdot}365} \tag{5.1}$$

and the corresponding relationship for rigid boundaries is:

$$Nu = 1{\cdot}56\,(R/R_c)^{0{\cdot}296} \tag{5.2}$$

according to Fromm (1965) and Clever and Busse (1974). In both cases, a Prandtl number of the order of unity and the critical value α_c of the wavenumber has been assumed. It is likely that more accurate calculations will slightly increase the exponent in expression (5.2), since the numerical approximations tend to underestimate the heat transport at high Rayleigh numbers.

The theoretical expression (5.2) appears to be in close agreement with experimental relationship (4.2(*c*)). But this apparent agreement is misleading. At Rayleigh numbers of the order of 10^5–10^8, for which calculated as well as measured Nusselt numbers have been obtained, the physically realised convection is turbulent and the two-dimensional structure has completely disappeared. In addition, the characteristic wavelength exceeds the critical value by nearly an order of magnitude. The decrease of the heat transport caused by the increasing wavelength is compensated by the small-scale motions in the boundary layers such that the observed heat transport approaches the theoretical value based on steady two-dimensional motion.

A direct comparison between computed values of the heat transport and measured ones has been done only at low Rayleigh numbers. By taking into account the observed variation of the wavelength of convection rolls, Willis *et al* (1972) were able to obtain good agreement between experimental data and theoretical predictions.

Although two-dimensional steady convection shows little relationship to observed convection at Rayleigh numbers in excess of 22 600 (see §6.1), the qualitative aspects of the numerical results are of considerable interest. The dependence of the heat transport on the Prandtl number is the most interesting property. In figure 7 the Nusselt number Nu is plotted as a function of P for different values of R. While the small-amplitude theory for rigid boundaries predicts that $Nu-1$ increases quadratically with P for small values of P and approaches its maximum value for $P\to\infty$, the computations at higher Rayleigh numbers indicate a maximum of Nu at a Prandtl number of the order of unity. In the case of the free boundaries, the value $Nu-1$ given by the first term of the series expansion (3.2) is independent of P, a feature which appears to be nearly preserved at high Rayleigh numbers, as indicated by figure 7. The slight decrease of Nu at the transition from the low Prandtl number regime to the high Prandtl number regime is caused by the disappearance of the momentum advection effect at high Prandtl numbers. The Prandtl number separating the two regimes increases proportional to $R^{2/3}$ according to Moore and Weiss (1973).

Even with the most advanced computers the computation of three-dimensional convection flows is only barely feasible. Computation costs are usually too high to permit systematic investigations of the problem and the research has thus been restricted to specific examples. The study by Lipps (1976) on time-dependent convection in air at Rayleigh numbers of the order of 10^4 represents the most detailed computation of three-dimensional convection to date.

5.2. Inertial convection

The dependence of the heat transport on the Prandtl number for low values of P

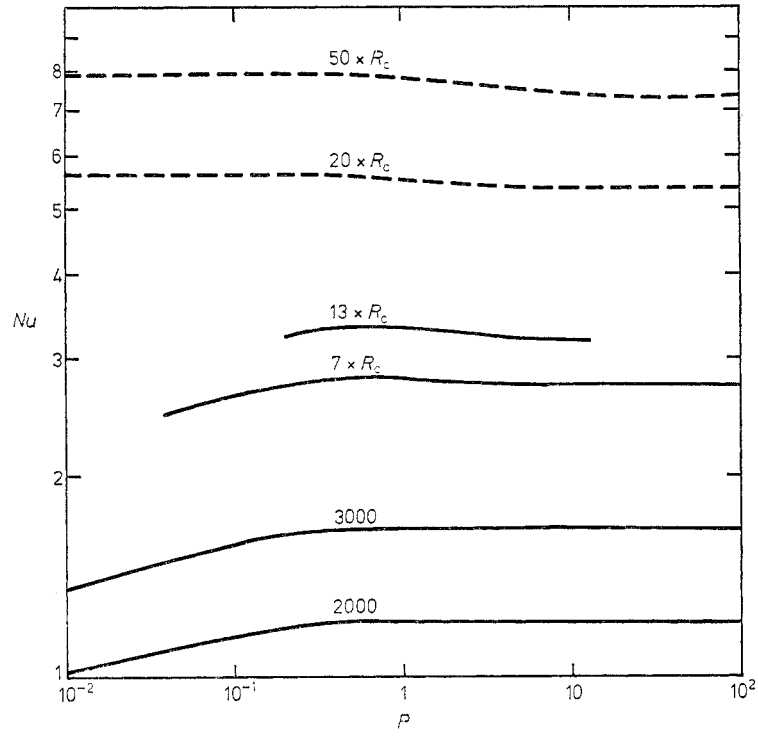

Figure 7. The Nusselt number of convection rolls as a function of the Prandtl number for different Rayleigh numbers indicated in the figure. Full lines corresponding to rigid boundaries ($\alpha = \alpha_c$) are plotted from numerical data by Plows (1971) and Clever and Busse (1974), broken lines corresponding to stress-free boundaries ($\alpha = 1$) represent data of Moore and Weiss (1973).

has long been a subject of strongly divergent opinions. The weakly non-linear theory predicts a P^2 dependence for rigid boundaries as well as for free boundaries, with the sole exception of the two-dimensional solution for which the heat transport becomes independent of P (Schlüter *et al* 1965). This unsatisfactory result of the weakly non-linear theory is due to the decreasing radius of convergence in the limit $P \to 0$. Indeed, the convective heat transport given by $Nu - 1$ in figure 7 increases much faster at low Prandtl numbers than at high ones, once the Rayleigh number exceeds the critical value by a finite amount. In an interesting numerical analysis of axisymmetric convection in a cylindrical box with stress-free boundaries, Jones *et al* (1976) actually found a distinct change from a solution with $\mathrm{d}Nu/\mathrm{d}R \propto P^2$ to a solution with $\mathrm{d}Nu/\mathrm{d}R \propto P^0$ at a Rayleigh number exceeding the critical value by 33%. This new Rayleigh number, called the effective critical Rayleigh number, assumes the role of the critical Rayleigh number at low Prandtl numbers, at least as far as the heat transport is concerned.

The physical origin for the sudden change in the effectiveness of the convective heat transport lies in the role of the inertial terms. The preferred solution becomes capable of balancing the term $\boldsymbol{u}.\nabla\boldsymbol{u}$ entirely by the pressure gradient in place of a partial balance with viscous friction. Physically this means that the convective motion assumes a 'flywheel' character, i.e. only a small fraction of the kinetic energy is lost by viscous dissipation in each period of circulation and the demand on the release of

potential energy is correspondingly small. Proctor (1977) has analysed this process analytically in the case of a horizontal cylinder heated from below. With stress-free boundaries, a convective motion in the form of rigid rotation could assume infinite speed because of the absence of viscous dissipation. With rigid boundaries, however, convection occurs first in the form of slow viscously dominated motions until, 7% above the critical Rayleigh number, the effective critical Rayleigh number is reached where the 'flywheel'-type motions can be realised. Interesting problems are posed by the questions whether the effective critical Rayleigh number represents a general phenomenon of low Prandtl number convection and whether similar effects do occur in the case of time-dependent three-dimensional convection. The relative high heat transport observed by Rossby (1969) for convection in mercury, which becomes time-dependent at low Rayleigh numbers (see figure 5), indicates an affirmative answer for the second question.

5.3. Boundary layer analysis

The difficulty of obtaining asymptotic expressions for the dependence of the heat transport on the Rayleigh number from mathematical analysis has led to the proposals of relationships based on heuristic arguments. Priestley (1954) has argued that the heat transport in high Rayleigh number convection should be independent of the depth of the layer because the heat transport is controlled by the thermal boundary layers adjacent to the upper and lower plates, while in the interior the convective heat transport is so efficient that it is not affected by the separation of the plates. Since the dimensional heat transport H^* is given by:

$$H^* = \frac{T_2 - T_1}{d} \rho_0 \kappa c Nu$$

H^* becomes independent of d if Nu is proportional to $R^{1/3}$. Other dimensional arguments are used in the astrophysical context (Spiegel 1971) where it is assumed that H^* is independent of the molecular diffusivities ν and κ with the consequence that Nu becomes proportional to $(RP)^{1/2}$. Stellar convection may indeed obey a different law for the heat transport, since the constraining effect of boundaries is much reduced in stars. But at the same time the discrepancy between different heuristic arguments emphasises their arbitrariness. The shortcomings of the arguments become evident when they are applied to the theoretical problems discussed in §§5.4 and 5.5 for which actual asymptotic solutions are available.

More satisfactory are arguments based on the instability of the thermal boundary layers. Since the mean temperature develops steep gradients near the boundaries where the heat is transported by conduction alone, and since the vertical velocity vanishes in those regions, it seems appropriate to apply the criterion (2.4) for the instability of a static state to the boundary layers. Using δ as the ratio between the boundary layer thickness and the depth of the convection layer (see figure 8), and taking into account that the mean temperature drops by about $\frac{1}{2}(T_2 - T_1)$ across the boundary layer, the criterion for instability becomes:

$$\tfrac{1}{2} R \delta^3 \geqslant R_c. \tag{5.3}$$

We note that this criterion is, to a first approximation, independent of the horizontal velocity at the boundary since it is well known (Deardorff 1965) that a mean horizontal shear does not affect criterion (2.4). Because heat is transported by conduction in the

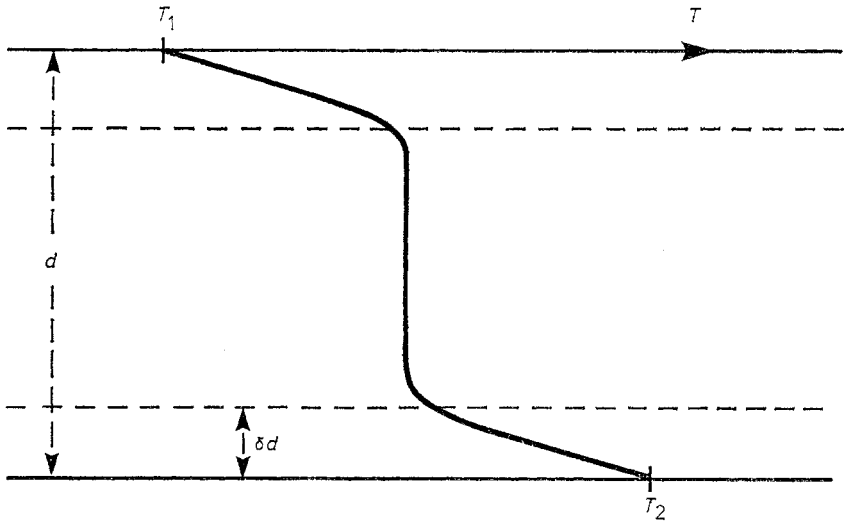

Figure 8. The profile of the horizontally averaged temperature. δ is the dimensionless thickness of the thermal boundary layers.

boundary layer, δ can be expressed in terms of the dimensionless heat transport H:

$$H = R/2\delta.$$

Thus the criterion for instability becomes:

$$H \leqslant \tfrac{1}{2} R(R/2R_c)^{1/3} \tag{5.4}$$

suggesting that the boundary layer is unstable unless the heat transport grows proportional to $R^{4/3}$. The fact that the heat transport by convection rolls in the presence of rigid boundaries grows at a slower rate is the basic reason for the instabilities of convection rolls for $R \geqslant 2{\cdot}3 \times 10^4$ (see §6). On the other hand, no instability has been found in the presence of stress-free boundaries (Straus 1972) where the heat transport grows at least proportional to $R^{4/3}$.

More detailed time-dependent models for the disruption of the thermal boundary layers by periodic instabilities have been developed by Chang (1957) and Howard (1966). These models yield a Nusselt number dependence proportional to $R^{1/3}$ and suggest the occurrence of oscillations with a frequency proportional to $R^{2/3}$ which appears to match frequencies observed in convection layers with moderately high Prandtl numbers.

The success of numerical computations of two-dimensional convection at high Rayleigh numbers has stimulated attempts to derive asymptotic solutions of equations (2.6) by boundary layer methods. As part of the analysis, asymptotic expressions for the heat transport can be obtained. In the case of stress-free boundaries the analysis is relatively easy and different investigators agree on a $R^{1/3}$ power law for the Nusselt number. But in the case of rigid boundaries the proposed power laws range from $R^{1/5}$ to $R^{1/3}$. For detailed discussions of the subject we refer to the papers by Roberts (1978), Robinson (1969) and Wesseling (1969). Like the numerically obtained two-dimensional solutions, the boundary layer solution does not give a physically realistic description of thermal convection at high Rayleigh numbers and the derived power laws for the heat transport are primarily of mathematical interest. But the dynamic

balances derived for the horizontal and vertical boundary layers provide the elements for the understanding of turbulent convection. In particular, the role of the Prandtl number and the wavelength of convection in non-linear thermal convection can be illuminated by boundary layer analysis and more refined solutions of the problem would be of considerable interest.

5.4. Mean field theories

The Rayleigh numbers of thermal convection in the atmosphere and in the hydrogen convection zones of stars are huge by comparison with those achievable in laboratory experiments. The importance of convection in many problems of astrophysics and meteorology has motivated the search for methods capable of giving good estimates for average properties of convection at very high Rayleigh numbers. Mixing length theories are commonly used for this purpose, but since they are based on heuristic statistical arguments they will not be considered here. A detailed discussion of turbulent convection based on the mixing length theory has been given by Kraichnan (1962) and for a recent review of the theory in the astrophysical context, we refer to Gough (1977).

An alternative approach to avoid the mathematical complexities of the complete set of equations (2.6) is to use a simplified version of those equations. The small-amplitude theory of convection indicates that the strongest non-linear effect arises from the modification of the horizontally averaged temperature distribution by the convective heat transport. It thus seems reasonable to neglect all other non-linear interactions in a first approximation and to consider the system of equations:

$$\nabla^2 \boldsymbol{u} + \theta \boldsymbol{\lambda} - \nabla \pi = 0 \qquad (5.5(a))$$

$$\nabla . \boldsymbol{u} = 0 \qquad (5.5(b))$$

$$\nabla^2 \theta - \boldsymbol{u} . \boldsymbol{\lambda} \boldsymbol{\lambda} . \nabla \Theta = 0 \qquad (5.5(c))$$

$$\boldsymbol{\lambda} . \nabla \Theta = \overline{\boldsymbol{u} . \boldsymbol{\lambda} \theta} - \langle \boldsymbol{u} . \boldsymbol{\lambda} \theta \rangle - R \qquad (5.5(d))$$

where the bar indicates the horizontal average and the brackets $\langle \ldots \rangle$ denote the average over the entire fluid layer. Θ is the mean temperature field which depends only on the z coordinate in the direction of $\boldsymbol{\lambda}$. In addition to the neglect of non-linear terms in the equations of the fluctuating variables, the time derivatives have been omitted since it can be shown (Spiegel 1962) that the system (5.5) does not admit oscillatory solutions. If the horizontal average is formally identified with an ensemble average, the mean-field approximation is equivalent to the third-order cumulant discard assumption for the closure of the statistical moment equations, as Herring (1963) has emphasised.

Herring (1963, 1964) solved equation (5.5) numerically in the case when the horizontal dependence is described by a single horizontal wavenumber. This numerical result for the dependence of the Nusselt number on the Rayleigh number agrees reasonably well with the subsequent boundary layer treatment of equations (5.5) by Howard (1965), in the case of free boundaries, and by Roberts (1966) and Stewartson (1966), in the case of rigid boundaries. When the wavenumber α is chosen such that the Nusselt number is maximised, the asymptotic relationships become:

$$Nu = 0{\cdot}325\, R^{1/3} \qquad \text{for stress-free boundaries} \qquad (5.6)$$

and

$$Nu = 0{\cdot}24\, (R^{3/2} \ln R^{3/2})^{1/5} \qquad \text{for rigid boundaries.} \qquad (5.7)$$

By investigating the stability of his single-α solution, Herring found indications that a solution of equation (5.5) with two horizontal wavenumbers is preferred for Rayleigh numbers above 10^6. Chan (1971) could indeed show, by applying the multiple boundary layer technique (see §5.5), that the maximum Nusselt number is reached asymptotically by a solution involving an infinite number of horizontal wavenumbers leading to a $R^{1/3}$ law in the case of rigid boundaries.

Since equation (5.5(a)) becomes identical to equation (2.6(a)) in the limit of infinite Prandtl number, it must be expected that the mean-field theory is most realistic in the case of large Prandtl numbers. Since it neglects the momentum advection terms which tend to enhance the heat transport at high Rayleigh numbers, it is not surprising that the exponent in relationship (5.6) is less than that of the numerically derived expression (5.1).

The mean-field equation (5.5) can be regarded as the most severe truncation in a hierarchy of truncations of the horizontal interactions between different modes. The next level of truncation is obtained when three horizontal wavevectors are included and interactions of the type (3.10) considered in the case of the hexagon solution are taken into account. This truncation has the advantage that it restores the Prandtl number as a parameter of the problem. Roberts (1966) was the first to analyse the resulting equations and a boundary layer analysis has been given by Gough *et al* (1975) which has been supplemented more recently by extensive numerical computations (Toomre *et al* 1977), ranging up to Rayleigh numbers of the order of 10^{20}. The results show that the Nusselt number depends only on the product PR in the limit $P \to 0$, which is a desirable feature from the astrophysical point of view, since the viscosity in stellar atmospheres is so small that it is widely believed among astrophysicists that it does not affect the Nusselt number. But as the discussion of inertial convection indicates, the limit of vanishing Prandtl number is not a simple one and the strong divergence in this limit between the result based on equations (5.5) and the next higher level of truncation suggests that quite different dependencies for the Nusselt number may be obtained when the interaction between different horizontal modes is taken into account more accurately.

5.5. The optimum theory of convection

The disadvantage of the results derived by mean-field theories is that the degree of approximation is not known unless experimental measurements or exact theoretical values are available for comparison. For many applications rigorous bounds on the convective heat transport are more useful than approximate results, especially if the bounds happen to be reasonably close approximations at the same time. Motivated by the earlier work of Malkus (1954b), Howard (1963) introduced the upper bound approach based on equations (2.6). Instead of calculating the heat transport for solutions of these equations, the maximum of the heat transport is determined among a manifold of fields $\boldsymbol{u}$, θ, which include all possible solutions of equations (2.6), which are statistically stationary in time. This maximum provides an upper bound for the heat transport of any physically realised convection flow under stationary conditions.

The maximum is obtained as the solution of a variational problem. The trial fields $\boldsymbol{u}$, θ share with the actual solutions of equations (2.6) the kinematic constraints expressed by conditions (2.6(b)) and (2.12) and the energetic constraints which are obtained by multiplying (2.6(a)) and (2.6(c)) by $\boldsymbol{u}$ and θ respectively, and averaging

the result over the fluid layer:

$$\langle \check{\theta} \boldsymbol{u}.\boldsymbol{\lambda} \rangle - \langle |\nabla \boldsymbol{u}|^2 \rangle = 0 \tag{5.8}$$

$$\langle \boldsymbol{u}.\boldsymbol{\lambda} \check{\theta} (\boldsymbol{\lambda}.\nabla\Theta) \rangle + \langle |\nabla \check{\theta}|^2 \rangle = 0. \tag{5.9}$$

As before, Θ denotes the horizontally averaged temperature and $\check{\theta}$ is the fluctuating component, $\check{\theta} = \theta - \Theta - Rz$. The boundary conditions (2.12) and the property that θ and $\boldsymbol{u}$ are bounded at infinity have been used to accomplish the partial integrations and to justify the neglect of terms which can be written in the form of surface integrals. In addition, it has been assumed that the time dependence of averaged quantities vanishes for statistically stationary turbulent convection.

By introducing expression (5.5(*d*)) for the mean temperature Θ and using the equality $\langle \phi(\phi - \langle\phi\rangle)\rangle = \langle(\phi - \langle\phi\rangle)^2\rangle$ relationship (5.9) can be rewritten:

$$\langle \overline{(\boldsymbol{u}.\boldsymbol{\lambda}\check{\theta} - \langle \boldsymbol{u}.\boldsymbol{\lambda}\check{\theta}\rangle)^2} \rangle + \langle |\nabla \check{\theta}|^2 \rangle - R\langle \boldsymbol{u}.\boldsymbol{\lambda}\check{\theta}\rangle = 0. \tag{5.10}$$

The variational problem is to find, at a given value of R, the maximum μ of $\langle \boldsymbol{u}.\boldsymbol{\lambda}\check{\theta}\rangle$ among all fields $\boldsymbol{u}$, $\check{\theta}$ that satisfy conditions (2.6(*b*)), (2.12), (5.8) and (5.10). Howard (1963) solved this problem in the case when the fields $\boldsymbol{u}$, $\check{\theta}$ are characterised by a single horizontal wavenumber and obtained an upper bound for the Nusselt number Nu which increased proportional to $R^{3/8}$ asymptotically. He also solved the variational problem without the constraint of the continuity equation (2.6(*b*)) in which case the upper bound increased proportional to $R^{1/2}$. Using a hierarchy of boundary layers, Busse (1969) solved the full variational problem by allowing for a countable number of horizontal wavenumbers and found that Howard's $R^{3/8}$ result is the first in the sequence of power laws describing the upper bound over finite ranges of the Rayleigh number and merging asymptotically into an $R^{1/2}$ law. The interesting feature of the upper bound curve is its similarity with the observed Nusselt number–Rayleigh number relationship. The upper bound exhibits kinks like those which have been observed by Malkus (1954a) (see §4.2) and even the locations of the kinks show approximate agreement, as the numerical confirmation of the analytical boundary results by Straus (1976) indicates. The transition in the upper bound from the $1-\alpha$ solution of Howard (1963) to the $2-\alpha$ solution of Busse (1969) is not unlike the transition to bimodal convection in that the second wavenumber characterises the horizontal dependence of a convection mode in the thermal boundary layers. But the physical basis for similarities at higher transitions is obscure since the time dependence of convection does not enter into the variational problem.

The mathematical methods of the optimum theory, as the upper bound approach has been called in the context of general turbulent transport problems, are discussed in detail in a recent review article (Busse 1978). The Euler–Lagrange equations of the variational problem are closely related to the mean-field equations (5.5). This similarity becomes even more pronounced if the limit of infinite Prandtl number is considered, in which case the constraint (5.9) can be replaced by the equation of motion (2.6(*a*)) itself. Chan (1971) has considered this problem and derived an asymptotic upper bound for the Nusselt number which increases proportional to $R^{1/3}$ and appears to be surprisingly close to the measured values. But the momentum advection terms neglected in the $P = \infty$ limit tend to enhance the heat transport as is evident from figure 6 and Kraichnan (1962) gives arguments suggesting an asymptotic $R^{1/2}$ dependence for the Nusselt number at moderate Prandtl numbers. Thus there seems to be not much room for a significant improvement of the general Prandtl number independent $R^{1/2}$ bound predicted by the optimum theory.

6. Instabilities of convection rolls

6.1. High Prandtl number fluids

The mathematical analysis of the instabilities of convection rolls was originally motivated by the observations of transitions in the patterns of convection and by the fact that the range of wavelengths realised in experiments is small compared to that predicted by linear theory. The comparison between theoretical predictions and experimental observations has shown that the analysis of instabilities can play a role beyond the original expectations. Since the transitions from two- to three-dimensional forms of convections often amount to relatively small modifications of the convection rolls, the linear analysis of the strongest growing disturbances is capable of describing most of the three-dimensional features of convection beyond the transition. Thus the combination of the numerical solution of steady two-dimensional convection and the analysis of its instabilities goes a considerable way towards a full description of three-dimensional convection.

The question of the realisable range of wavelengths of convection rolls can be addressed already on the basis of the weakly non-linear theory discussed in §3 (Schlüter *et al* 1965, Busse 1971). There are two main instability processes which prevent the realisation of rolls with wavenumbers α beyond a certain range in the neighbourhood of α_c. When the wavenumber of the roll is small, the zig-zag instability occurs, which induces wavy distortions of the rolls, as shown in figure 9(*a*) (plate). By lengthening the boundary between the rolls, it effectively decreases the wavelength of the rolls. Experiments by Busse and Whitehead (1971) show that rolls with an angle of about 45° to the original roll pattern tend to be established as final state, with wavenumbers close to the critical value α_c. The instability mechanism which prevents the realisation of rolls with a short wavelength is not quite as elegant, but no less effective. The cross-roll instability occurs in the form of rolls at a right angle to the original pattern as shown in figure 9(*b*) (plate). The theoretical predictions shown in figure 10 are in good agreement with the experimental observations in high Prandtl number fluids. At Prandtl numbers of the order of unity or less, the cross-roll instability is replaced by the two-dimensional Eckhaus instability (see the discussion by Busse (1971)), but no experimental observations of this instability have yet been made.

At higher Rayleigh numbers the wavelength of the growing cross-roll disturbances becomes smaller than that of the original roll pattern and instead of a final state of two-dimensional rolls the three-dimensional state of bimodal convection is established (figure 11 (plate)). Beyond $R_{II}=22\,600$ convection in the form of two-dimensional rolls cannot be realised in large Prandtl number fluids. The origin of the transition to bimodal convection lies in the instability of the thermal boundary layer as was pointed out in §5.3 and the predominance of the secondary roll in the boundary layers (Busse 1967b) confirms this interpretation.

Figures 9, 11 and 15 (plates) show shadowgraph visualisation of convection in a layer heated from below. A schematic sketch of this experimental technique which was first used by Chen and Whitehead (1968) is given in figure 12. The temperature dependence of the refractive index causes slight deflections when a nearly parallel beam of light traverses the convection layer. Accordingly, the pictures indicate the horizontal pattern of the vertically averaged temperature in the layer. A second feature of these experiments (see Busse and Whitehead (1971) for a more detailed description) is the use of controlled initial conditions. By generating small two-dimensional temperature perturbations before the Rayleigh number of the convection

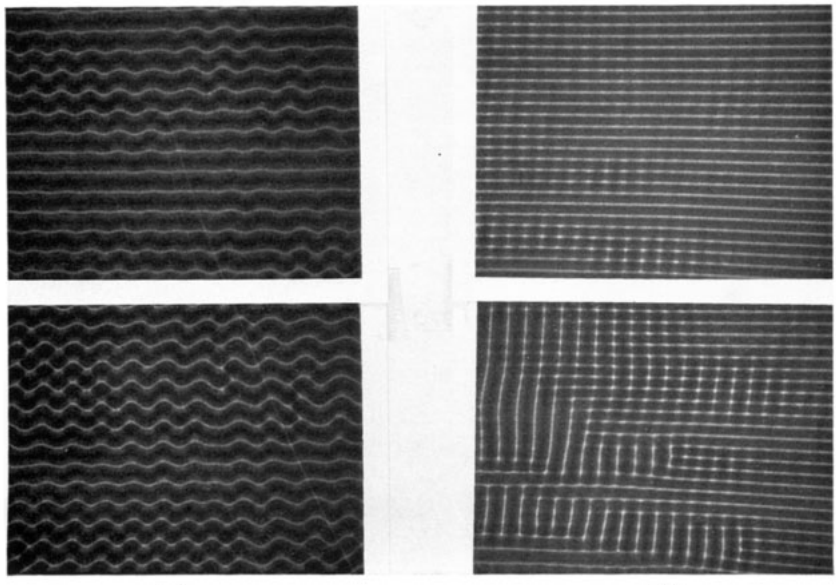

(*a*) (*b*)

Figure 9. Instabilities of convection rolls in a fluid layer with $P \sim 100$: (*a*) zig-zag instability, (*b*) cross-roll instability. For further details see Busse and Whitehead (1971).

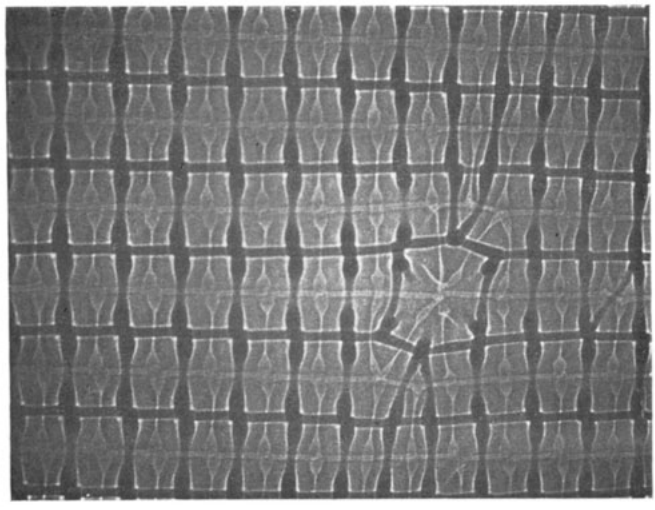

Figure 11. Pattern of bimodal convection with an imperfection for $P \sim 100$, $R \sim 5 \times 10^4$.

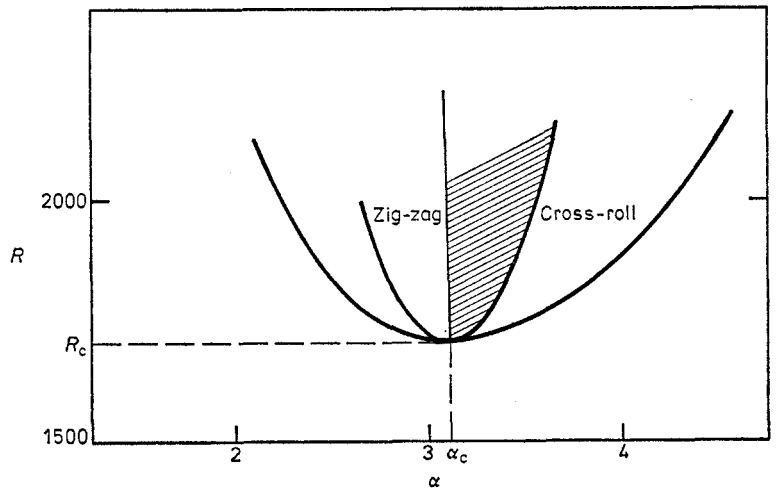

Figure 10. Region of stable convection rolls (shaded) near the critical Rayleigh number for large Prandtl number. The lower curve gives $R(\alpha)$ from linear theory.

layer is raised above the critical value, rolls with a prescribed wavelength can be induced. Thus the predictions of theory can be tested with a much higher degree of accuracy than in experiments with uncontrolled initial conditions. The laboratory observations have been found in good agreement with the theoretical predictions for Prandtl numbers of the order of 5 and higher which are accessible by the experimental method.

6.2. Low Prandtl number fluids

While the stability properties of large Prandtl number convection depend on the non-linear term in the heat equation (2.6(*c*)), the non-linear momentum advection

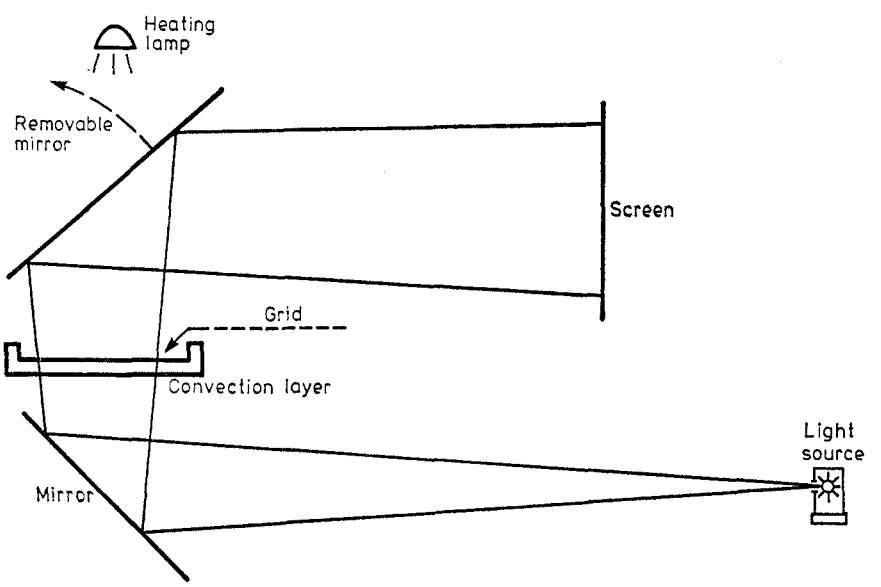

Figure 12. Schematic sketch of the shadowgraph visualisation method and the technique of producing controlled initial condition in the convection layer.

terms of the equation of motion (2.6(a)) play a dominant role in low Prandtl number instabilities of convection. By considering convection rolls in the case of stress-free boundaries it is possible to develop an analytical stability theory in the limit of vanishing Prandtl number (Busse 1972). In this limit the instability of convection rolls occurs in the form of oscillations which propagate along the rolls as shown in figure 5. Since the critical Rayleigh number R_{III} for the onset of oscillations is given by $R_{\mathrm{III}} = R_c + AP^2$ for small P the stability range of stationary rolls vanishes for $P \to 0$. In the case of rigid boundaries, numerical methods must be applied to determine the stability region of convection rolls. The results of Clever and Busse (1974) indicate that a small but finite region where stationary rolls are stable remains in the limit of vanishing Prandtl number.

Because of their particular symmetry, two-dimensional convection rolls do not have a vertical component of vorticity. From the equation of motion it can also be seen that arbitrary three-dimensional convection cannot acquire a vertical component of vorticity in the limit of infinite Prandtl number. The oscillatory instability is characterised by a strong component of vertical vorticity and thus represents the main mechanism in which this degree of freedom of motion is occupied in the development of turbulent convection. The influence of the vertical component of vorticity on the non-linear properties of convection is not well understood. The numerical computations of time-dependent convection in air by Lipps (1976) indicate a decrease of $\mathrm{d}Nu/\mathrm{d}R$ at the onset of the oscillatory instability at $R \sim 5 \times 10^3$, but experimental evidence suggests that an increase occurs at somewhat higher values of R of the order of 8×10^3.

Another feature of oscillatory convection that is of interest, from the point of view of the general theory of turbulence, is the transition to an aperiodic time dependence. In extending the linear stability analysis, McLaughlin and Martin (1975) analysed the non-linear interaction of several modes of oscillation and found an aperiodic time dependence for four interacting modes. They interpret this result as an example of the sudden transition to turbulence which occurs according to Ruelle and Takens (1971) after no more than three bifurcations to periodic or quasi-periodic states have taken place. This hypothesis contradicts the traditional view that the transition to turbulence occurs gradually in cases such as convection, by a series of bifurcations to increasingly complex states of fluid flow. More detailed computations will be required to clarify the onset of aperiodic time dependence in convection and to demonstrate that the results do not depend on the particular choice of truncation in the modal expansion.

6.3. Intermediate Prandtl number fluids

The problem of determining the boundaries of the region of stable convection rolls in the R–α plane becomes more complex at intermediate Prandtl numbers because, in addition to the mechanisms of instability mentioned above, two additional mechanisms must be considered, both of which disappear in the limits of small as well as large Prandtl numbers. The numerical computations by Clever and Busse (1974, 1978) and Busse and Clever (1978) have been carried out only for selected values of P. But by combining the stability diagrams into the three-dimensional graph shown in figure 13, a fairly complete picture of the stability region of convection rolls evolves.

The predominant instability at Prandtl numbers of the order of unity is the skewed varicose instability which tends to distort the roll pattern in the way shown in figure 14.

It does not lead to a new form of convection, but instead transforms the rolls into rolls of larger wavelength, as is indicated by the experimental observations (Busse and Clever 1978). The fact that the characteristic wavelength of convection increases with increasing Rayleigh number has long been a puzzling experimental result, especially in fluids with moderate Prandtl numbers, such as air. The hypothesis that wavelengths corresponding to a maximum heat transport are preferred suggests that the wavelength should decrease rather than increase with increasing Rayleigh number in contrast to the experimental evidence. Contrary to this idea, the skewed varicose

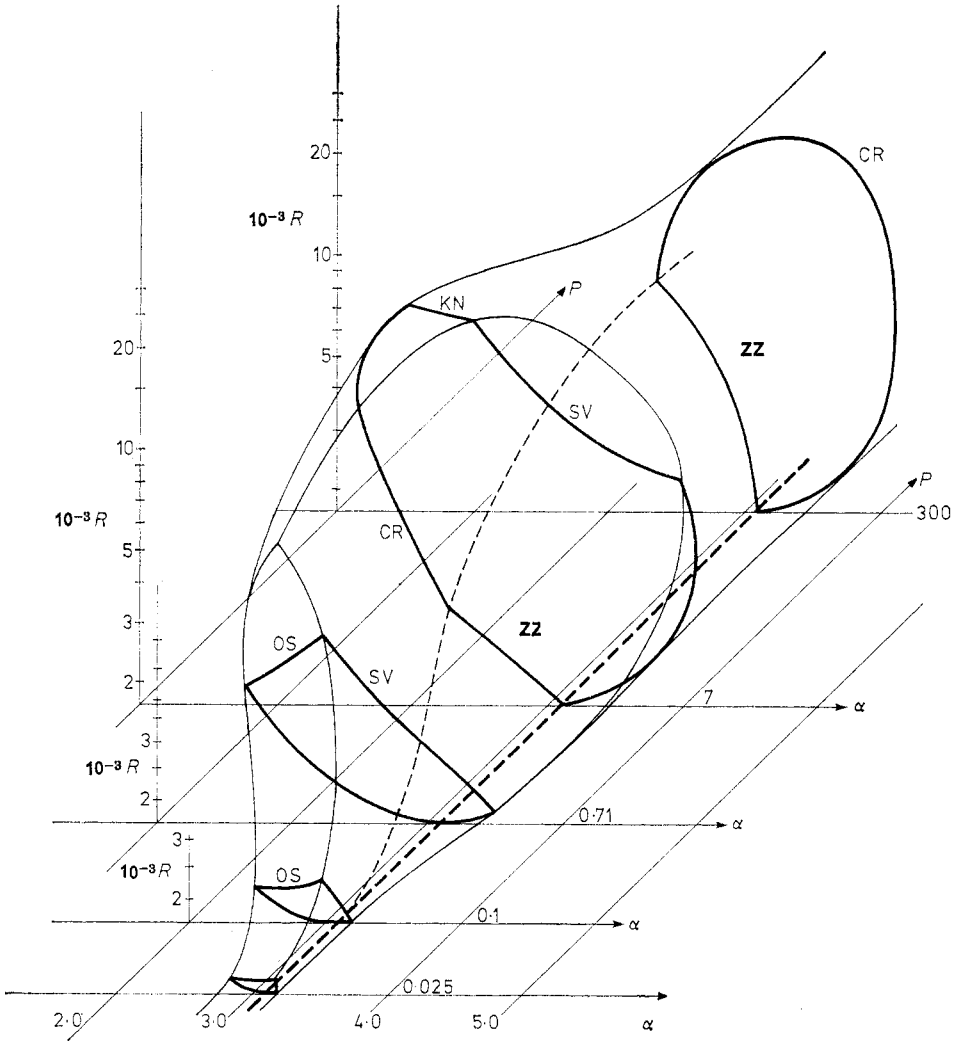

Figure 13. Region of stable convection rolls in the three-dimensional R–P–α space. The thick curves represent computed stability boundaries for the oscillatory (OS), the skewed varicose (SV), the cross-roll (CR), the knot (KN), and the zig-zag (ZZ) instabilities. The other curves represent approximate interpolations from results of Busse and Clever (1978). The stability boundary for $P=300$ actually represents the computations of Busse (1967b) for $P=\infty$ which are expected to give a good approximation for $P=300$.

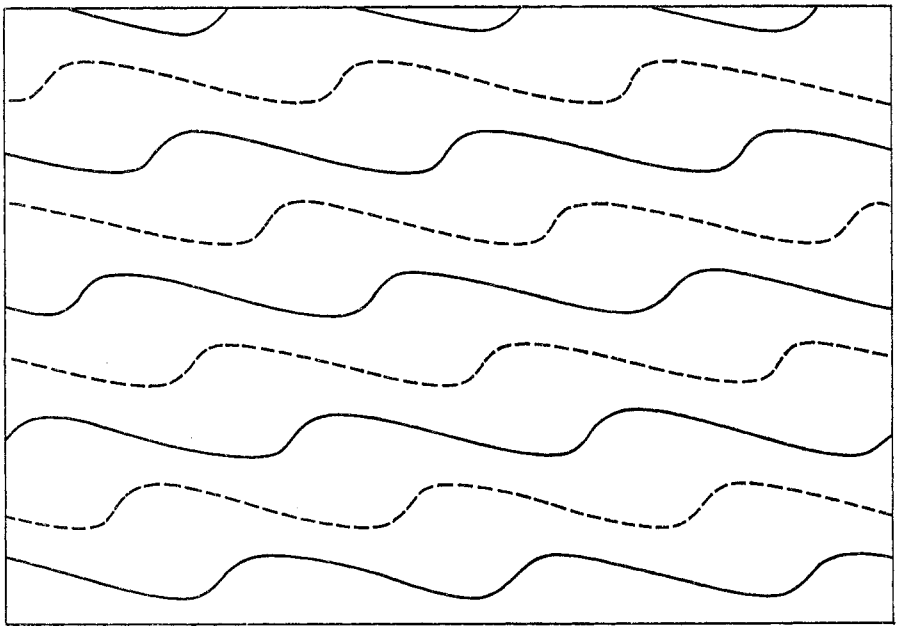

Figure 14. Qualitative sketch of the distortion of a horizontal pattern of convection rolls by the skewed varicose instability. Full and broken lines indicate approximately the maxima of up- and down-going motion.

instability which originates from an interaction of the non-linear terms in the equation of motion and the heat equation causes a shift towards larger wavelength in good agreement with the experimental data (Clever and Busse 1978).

The other new instability at intermediate Prandtl numbers is the knot instability, which may be regarded as a modification of the cross-roll instability. In contrast to the latter, the wavelength of the knot instability is much larger than $2\pi/\alpha_c$ and instead of a new roll pattern at right angles to the original one, a spoke pattern form of convection is introduced, as shown in figure 13. This kind of convection is organised in large-scale cells which are nearly steady and small-scale spoke-like sheets of hot and cold fluid which erupt from the lower and upper thermal boundary layer, respectively. The 'spokes' exhibit a highly fluctuating time dependence on the time scale of convective circulation time. In general, the spokes tend to move towards the spoke centre.

The spoke pattern cells have some similarity with the hexagonal cells discussed in §3.3 and 4.1. In contrast to the latter, spoke pattern cells occur under symmetric conditions and cells with rising and descending motion at the centre are both realised at the same time. At Rayleigh numbers of the order of 10^5–10^7, spoke pattern convection represents the dominant form of convection over a wide range of Prandtl numbers as has been discussed in §4.3.

The transition from rolls to spoke pattern convection occurs through the intermediate stages of bimodal convection and oscillatory bimodal convection for Prandtl numbers larger than about 10, depending on the wavelength. Indications for the competition between the knot instability and the small-scale cross-roll instability leading to bimodal convection can be seen at a Prandtl number of 7, as shown in figure 15 (plate). The oscillatory instability of bimodal cells occurs in a similar way as the oscillatory instability of rolls, except that only standing waves are permitted by the three-dimensional nature of the basic pattern. The theoretical dispersion relation can

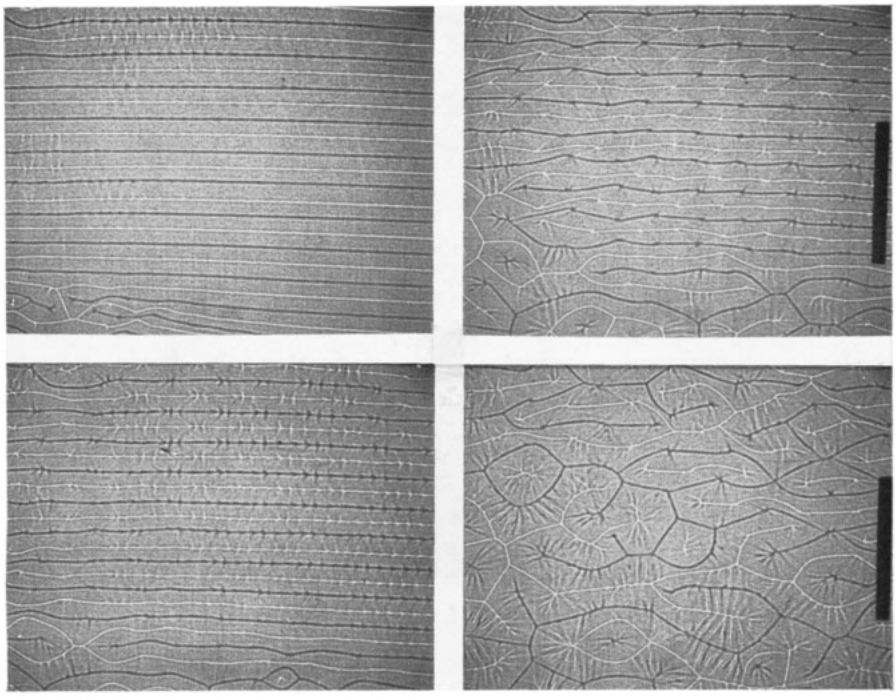

Figure 15. Onset of knot and cross-roll instabilities. The latter is characterised by a small wavelength and disappears soon. The convection fluid is methyl alcohol, with a Prandtl number of 7, and the Rayleigh number is approximately $2{\cdot}1 \times 10^4$.

be applied with good success and even the critical Rayleigh number for the onset of oscillations (given by the upper boundary of the shaded region in figure 5) represents a continuation of the theoretical curve of Clever and Busse (1974) into the domain of bimodal convection. The instability leading from oscillatory bimodal convection to spoke pattern convection has been called collective instability in an earlier paper (Busse and Whitehead 1974), but it appears to represent essentially the same mechanism as the knot instability. Thus the results of the stability analysis in the case of rolls turns out to be useful for the interpretation of transitions occurring in the more complex forms of three-dimensional convection.

7. Convection in rotating systems

7.1. General discussion

Convection processes of geophysical and astrophysical interest usually occur in rotating systems. The Earth's rotation has relatively little effect on atmospheric convection because the circulation time of the latter, measured in terms of hours, at most, is small compared to the period of rotation. But in the Earth's core the influence of rotation is much more significant because of the larger length scales. Similarly convection in the solar atmosphere shows no measurable effect of rotation on the granulation scale, but noticeable influence on the scale of the supergranulation, and the dynamics of the giant cells, representing the largest scale of convection in the Sun, appears to be dominated by the Coriolis force.

Convection in a rotating system is of special interest because it exhibits some non-linear phenomena which do not occur in a non-rotating system. The most important is the generation of mean flows in the form of a differential rotation by the action of the Reynolds stresses of the convective motion. The appearance of unusual forms of instability also seems to be a peculiarity of rotating systems. Because of the larger experimental effort required for laboratory investigations, convection in a rotating system has not yet received the attention it deserves. Perhaps the interesting phenomena mentioned in the following will stimulate some further research.

Any discussion of nearly steady motions in a rotating system must start with the fundamental dynamic constraint known as the Proudman–Taylor theorem. Since only the pressure gradient can balance the Coriolis force in the limit when the viscosity and the amplitude of motions are small, the curl of the Coriolis force must vanish. This requires the Proudman–Taylor condition:

$$\boldsymbol{\Omega}.\nabla\boldsymbol{u}=0 \tag{7.1}$$

i.e. the velocity field $\boldsymbol{u}$ must not depend on the coordinate in the direction of the angular velocity vector $\boldsymbol{\Omega}$.

Two different cases of convection can be distinguished in a rotating system depending on the inclination of the convection layer with respect to the vector $\boldsymbol{\Omega}$. When the layer is parallel to $\boldsymbol{\Omega}$, convection rolls aligned with the axis of rotation can satisfy condition (7.1) and the Coriolis force can be balanced by the pressure gradient. In these ideal circumstances, convection occurs in the same way as in a non-rotating system, except for the alignment and the associated loss of horizontal isotropy (see figure 16(*a*)). Deviations from the perfect validity of condition (7.1) are of great practical importance and are discussed in §7.3.

When the vector $\boldsymbol{\Omega}$ is inclined with respect to the convection layer, motions which

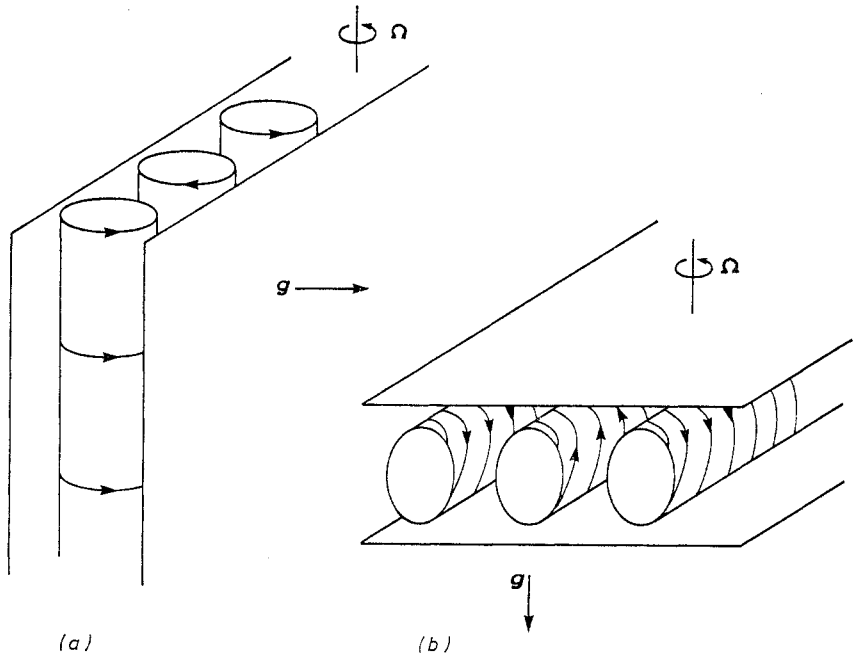

Figure 16. (*a*) Convection rolls in a layer rotating about a parallel axis are aligned with the axis. (*b*) Convection rolls in a layer rotating about a perpendicular axis.

satisfy both condition (7.1) and the condition that the normal velocity vanishes at the boundaries must be parallel to the boundaries of the layer and thus parallel to the isotherms of the basic state. Convective motions releasing potential energy must therefore violate condition (7.1). By decreasing the horizontal length scale of convection, viscous friction can become comparable to the Coriolis force and the constraint (7.1) can be avoided at the expense of a large increase of the critical Rayleigh number for the onset of convection. The principle example for this kind of balance is the problem of convection in a horizontal layer rotating about a vertical axis (see figure 16(*b*)).

7.2. Convection with a vertical axis of rotation

Convection in a layer heated from below and rotating about a vertical axis shares with the case of a non-rotating layer discussed in §3 the property of the degeneracy of the linear problem caused by the horizontal isotropy of the layer. In contrast to the non-rotating case, the onset of convection occurs in the form of an oscillatory mode when the Prandtl number is sufficiently small and the Taylor number is not too low. The latter is defined by:

$$T = 4\,\Omega^2 d^4/\nu^2 \tag{7.2}$$

and represents the square of the ratio between Coriolis and frictional force.

The degeneracy of the linear problem can be attacked in analogy to the non-rotating case by first considering the constraints imposed by the solvability conditions of the perturbation expansion for the non-linear problem and a subsequent stability analysis. Küppers and Lortz (1969) found that two-dimensional convection rolls

represent the only stable steady solution as in the non-rotating case. But for $T \geqslant T_c$, even the rolls are unstable according to Küppers and Lortz. For stress-free boundaries, T_c has the value 2285 at infinite Prandtl number and decreases slightly with decreasing P. Since oscillatory modes of convection are not possible for Prandtl numbers larger than unity, no steady or time periodic solution appears to be realisable in the neighbourhood of the critical Rayleigh number where the perturbation analysis is valid.

A more detailed inspection of the time-dependent problem reveals that an initially established pattern of rolls does indeed become unstable to disturbances in the form of rolls inclined with an angle of about 60° in the prograde direction with respect to the given rolls. As the disturbance rolls grow, the original rolls decay and the new roll pattern reaches the equilibrium amplitude of convection. At that point the instability process repeats itself with the new disturbance rolls appearing at an angle of about 120°. The time scale of this cyclic process of instability is certainly governed by the initial amplitudes of the disturbances. If it is assumed that the experimental noise can be described by a constant amplitude for all disturbances of a given wavenumber, the process of cyclic instability leads to solutions which are quasi-periodic in time (Busse and Clever 1979). For a more realistic description of the problem, statistical assumptions about the experimental noise must be introduced and accordingly the time dependence of the convection will acquire statistical properties. Thus the problem of convection in a rotating layer exhibits a basic property of turbulent systems in that at any one time a solution is realised among a manifold of possible solutions, all of which are unstable with respect to some other solution of the manifold.

The subcritical onset of finite amplitude convection is another non-linear phenomenon occurring in a rotating layer. Like the onset of oscillatory convection, and typically in close competition with it, subcritical steady finite amplitude convection takes place if the Prandtl number is sufficiently small. Although both phenomena are favoured by small Prandtl numbers, oscillatory convection and subcritical steady convection do not seem to have a direct physical connection. In contrast to the case of a negative contribution $\epsilon R^{(1)}$ in expression (3.2(*b*)) which is responsible for the subcritical hexagon solution displayed in figure 4, a negative value of $R^{(2)}$ is the cause of subcritical convection rolls in a rotating layer (Veronis 1959, Küppers 1970). The non-linear terms in the equation of motion are capable of partially releasing the constraint of the Coriolis force. In his measurements of the convective heat transport, Rossby (1969) finds that the release of the rotational constraint is so efficient at higher Rayleigh numbers that the heat transport is larger than in the non-rotating case in a certain range of Taylor numbers. Numerical computations (Veronis 1968) do not confirm this effect unless significant changes in the wavelength of convection are assumed (Somerville 1971). Thus it appears that the increase of the heat transport is mainly caused by the absence of instabilities, in a rotating layer, which tend to lengthen the wavelength of convection in a non-rotating layer.

7.3. Convection with a horizontal axis of rotation

Convection with a 'horizontal' axis of rotation can be easily realised in a laboratory experiment if the centrifugal force is used in the place of gravity. By rotating a cylindrical fluid annulus, cooled from within and heated from the outside, the configuration of figure 14(*a*) can be achieved. Even if the Earth's gravity is not small in comparison with the centrifugal force, it does not influence the convection when the

rotation axis is vertical. Since in this case the convection flow is perpendicular to the Earth's gravity, the latter does not contribute to the energy balance.

The top and bottom surface of the annulus cause some deviations from the Proudman–Taylor condition (7.1). When the two boundaries are parallel, the deviation is minimal because the velocity field adjusts to the boundary condition for the tangential component within a thin boundary layer of thickness $(\nu/\Omega)^{1/2}$. More interesting is the case of non-parallel conical surfaces, as shown in figure 17. Assuming that $\eta = \tan\phi$ is a small number and that the cylindrical boundaries of the annulus are stress-free, the Rayleigh number for the onset of convection rolls with the azimuthal wavenumber α becomes:

$$R(\alpha) = (\pi^2+\alpha^2)^3/\alpha^2 + [2\eta Pd/L(1+P)]^2\, T(\pi^2+\alpha^2)^{-1} \tag{7.3}$$

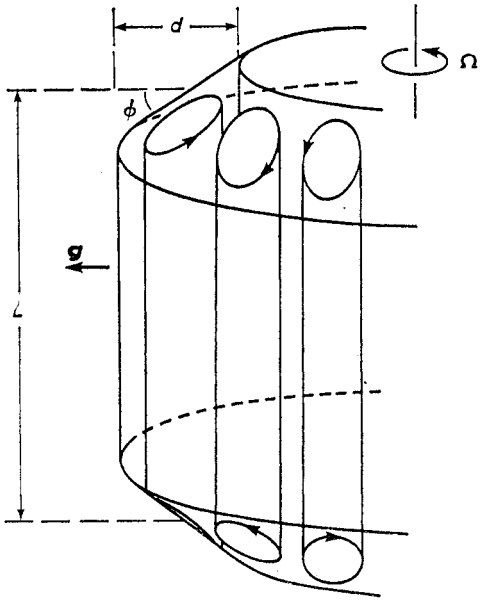

Figure 17. Convection in a rotating annulus with conical top and bottom boundaries.

in place of expression (2.10), where L is the height of annulus. When (7.3) is minimised with respect to α in the limit of large values of the Taylor number T, the minimising wavenumber grows proportional to $T^{1/6}$ and the critical Rayleigh number approaches the dependence:

$$R_c = 3[2\eta Pd/L(1+P)]^{4/3}(T/2)^{2/3}. \tag{7.4}$$

The more detailed analysis (Busse 1970a, Busse and Carrigan 1974) shows that the deviation from the Proudman–Taylor condition (7.1) causes a time dependence in addition to the increase of the azimuthal wavenumber. The convection columns propagate with a phase velocity proportional to $\eta\Omega$ in the prograde (retrograde) direction when the height of the annulus decreases (increases) with the distance from the axis.

Of particular interest for geophysical and astrophysical applications is the generation of a mean flow by the fluctuating convection velocity field. This process does occur when the angle ϕ of inclination becomes a function of the distance from the axis.

Using perturbation theory, it can be shown that the mean azimuthal component of the Reynolds stress does not vanish in this case, and a differential rotation proportional to the radial curvature of top and bottom boundaries is produced, as shown in figure 18. This effect, as well as the above-mentioned properties of the convection columns, can be measured in laboratory experiments (Busse and Carrigan 1974, Busse and Hood 1978) and good agreement with the theoretical predictions is generally found.

The annulus shown in figure 16 may be regarded as a cylindrical section of a sphere and, indeed, the theory developed for the annulus can be applied as a first approximation to the problem of convection in a rotating self-gravitating sphere heated from within (Busse 1970a). This application is possible because the criterion $R > R_c$ for convective instability given by expression (7.4) becomes independent of the thickness d of the annulus for a given temperature gradient, since the factor d^4 can be cancelled from both sides of the inequality $R > R_c$. The fact that gravity is directed inward instead of the outward pointing vector of figure 16 does not cause any difference as long as the temperature gradient is reversed at the same time. The property that only the product of temperature gradient and gravity vector enters the dynamics of the problem is the basis for the laboratory simulation of convection in rotating self-gravitating spheres using the centrifugal force (Busse and Carrigan 1976). Even though the angle of the inclination of the boundaries is of the order of unity in the case of the sphere, the laboratory observations are in reasonable agreement with the prediction of the perturbation theory. A more exact theoretical treatment of the problem of convection in a rotating sphere indicates that the perturbation approximation

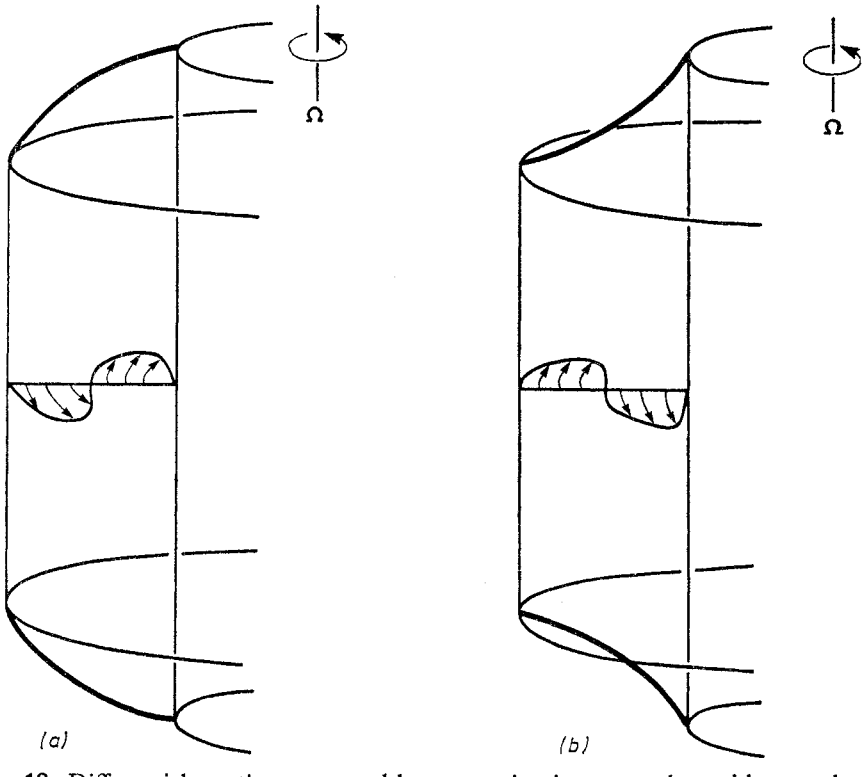

Figure 18. Differential rotation generated by convection in an annulus, with curved top and bottom boundaries.

corresponds to a non-linear solution which ceases to exist in the linear limit (Soward 1977).

Because of the latitudinal inhomogeneity of the heat transport, the non-linear properties of convection in a rotating sphere or in rotating spherical shells are complicated and require numerical computations (Gilman 1977). Only in the limit of thin spherical shells can relatively simple results be obtained for Taylor numbers T less than about $10^2 r_0/d$, where T is based on the thickness d of the shell and where r_0 is its radius. The experimental photograph (figure 19) (plate) gives a good picture of the convection realised in this case, which is described by the spherical harmonic $P_m^m(\cos\theta)\exp(im\phi)$. As in the case of the annulus with curved top and bottom surfaces (figure 18), the non-linear terms in the equation of motion lead to a non-vanishing mean Reynolds stress in the azimuthal direction which causes the fluid to rotate faster at the equator than at the poles.

When this effect was discovered, it presented itself as a natural explanation for the differential rotation of the Sun (Busse 1970b, 1973). The simple mathematical model describes the observed features of the solar differential rotation qualitatively correctly and fits the data even quantitatively if an appropriate eddy viscosity is introduced to take into account the effect of the small-scale turbulence of the solar convection zone. While confirming the analytical perturbation theory in the low Rayleigh number regime, the numerical computations by Gilman (1977) show the opposite phenomenon of a differential rotation increasing with latitude at higher Rayleigh numbers where the perturbation theory is no longer applicable. It thus seems that low Rayleigh number convection provides a better approximation for the highly turbulent convection systems encountered in the astrophysical and geophysical contexts. But before such a general statement can be made, a better understanding of the relationship between convection in stars and convection on laboratory scales is needed.

8. Concluding remarks

In selecting the examples of non-linear properties of thermal convection described in this review, the attention has been focused on those cases which correspond to the simplest physical conditions and which have been investigated in the greatest detail. The interesting non-linear effects exhibited by doubly diffusive convection processes, by penetrative convection and by convection in the presence of magnetic fields have not been mentioned, and for information the reader is referred to literature mentioned in the introduction, in particular the article of Spiegel (1972). Although a number of new phenomena occur when additional physical effects enter the problem of thermal convection, most of them can be understood by methods of analysis similar to those outlined in the preceding sections. Whenever non-linear processes dominate, as in most geophysical and astrophysical applications of convection theory, the simple case of a Boussinesq fluid layer heated from below provides the foundation on which more detailed models can be built.

The desire to understand convection processes observed in the Earth's atmosphere and on the surface of the Sun has long been a major motivation for the investigation of non-linear properties of convection. The discrete scales on which convection appears to occur in the Earth's as well as the solar atmosphere is perhaps the most puzzling phenomenon waiting for an explanation. On the Sun, three distinct modes of convection can be distinguished corresponding to granulation, supergranulation,

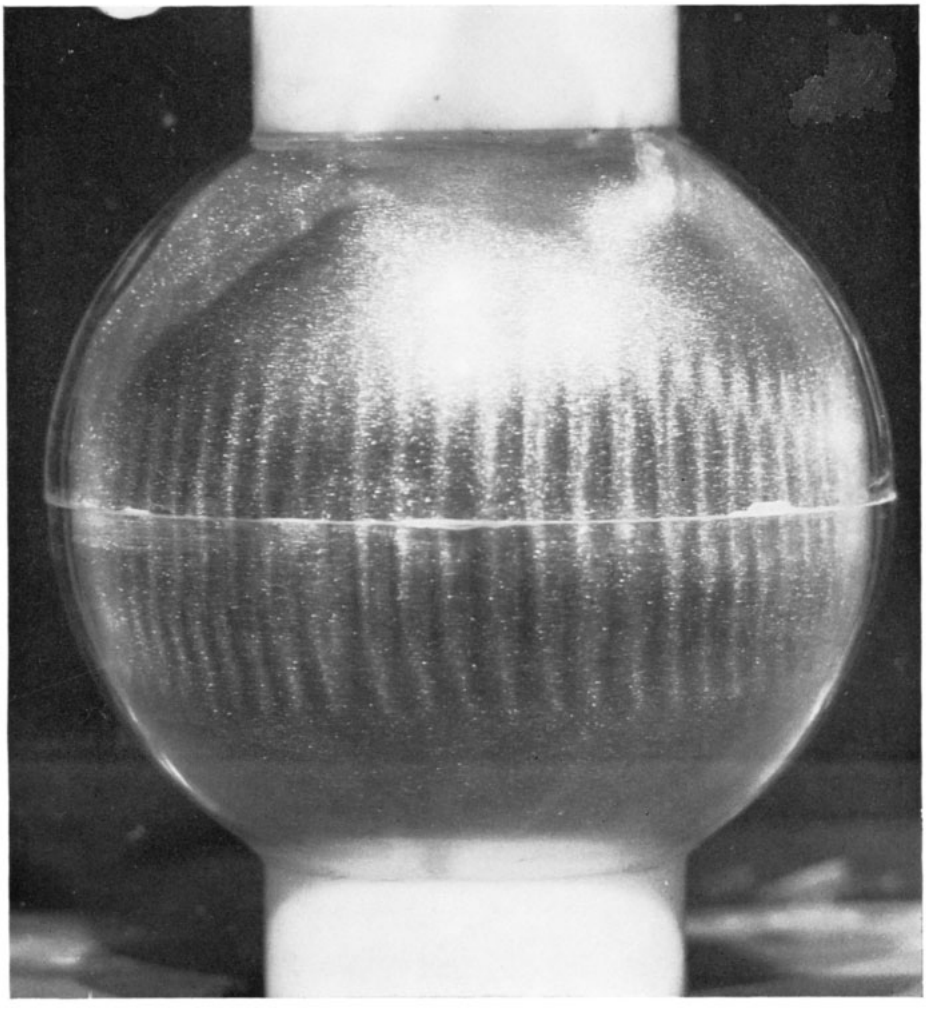

Figure 19. Convection in a rotating spherical shell of radius $r_0 = 5$ cm, with a gap width $d = 0{\cdot}32$ cm. The motion is made visible by a suspension of flaky particles which tend to align with the shear.

and giant cells separated by a factor of 10 in their horizontal scales. In the Earth's atmosphere convection cells become visible in the form of patterns of cumulus clouds and the horizontal scale varies from 100 m to nearly 100 km. The latter value is approached in the case of mesoscale convection whose surprisingly regular structure was discovered by satellite photography. Although observed cloud patterns exhibit rather well-defined wavelengths, it is not clear whether a similar hierarchy of scales exists as in the solar convection zone. The answer to this question is complicated by the fact that other atmospheric processes besides convection produce regular patterns of clouds.

The discrete scales exhibited by terrestrial and solar atmospheric convection are puzzling because they contradict the notion that the dynamics of turbulent fluids are governed by random processes in the limit of asymptotically high Rayleigh and Reynolds numbers. On the other hand, the custom of interpreting the similarity between atmospheric convection and laminar convection in laboratory experiments in terms of eddy diffusivities does not have a sound physical basis and does not do justice to the observed hierarchy of scales. If anything, the investigation of the instabilities of laminar convection and the transition to more complex forms of motion has made it more difficult to draw simple analogies between patterns observed in the laboratory and on an atmospheric scale. Thus there remains a broad gap between the non-linear processes that we have learned to understand at low Rayleigh numbers and the order that seems to emerge at very high values of this parameter.

That discrete structures in highly turbulent systems are most evident in the case of convection in the form of the kinks in the heat transport curve mentioned in §4.2 and in the form of discrete wavelengths is no accident. Other turbulent fluid systems usually do not offer the kind of information provided by the view of a two-dimensional pattern of convection as a function of time. Regular structures become apparent in this case which may remain unrecognised if properties are measured only at a few points as a function of time. Other advantages of thermal convection as a particularly simple realisation of turbulent fluid flow are the horizontal isotropy and the relatively simple energy source, which makes the problem more accessible to theoretical investigation. For these reasons it seems likely that thermal convection will become an even more important model for research on non-linear processes in fluid mechanics than it has been in the past.

Acknowledgments

The author gratefully acknowledges the support of his research on thermal convection by the Atmospheric Sciences Section of US National Science Foundation.

References

Ahlers G and Behringer R P 1978 *Phys. Rev. Lett.* **40** 712–6
Berge P 1975 *Fluctuations, Instabilities, and Phase Transitions* ed T Riste (New York: Plenum)
Busse F H 1962 *Das Stabilitätsverhalten der Zellular Konvektion bei endlicher Amplitude* (*Dissertation, University of Munich*) (Engl. trans. by S H Davis *Rand Rep.* LT-66-19 (Rand Corp, Santa Monica, California, USA))
—— 1967a *J. Fluid Mech.* **30** 625–49
—— 1967b *J. Math. Phys.* **46** 140–50
—— 1967c *J. Fluid Mech.* **28** 223–39
—— 1969 *J. Fluid Mech.* **37** 457–77

—— 1970a *J. Fluid Mech.* **44** 441–60
—— 1970b *Astrophys. J.* **159** 629–39
—— 1971 *Instability of Continuous Systems* ed H Leipholz (Berlin: Springer-Verlag) pp41–7
—— 1972 *J. Fluid Mech.* **52** 97–112
—— 1973 *Astron. Astrophys.* **28** 27–37
—— 1978 *Adv. Appl. Mech.* **18** 77–121
Busse F H and Carrigan C R 1974 *J. Fluid Mech.* **62** 579–92
—— 1976 *Science* **191** 81–3
Busse F H and Clever R M 1978 *J. Fluid Mech.* in press
—— 1979 *Springer Lecture Notes in Physics* in press
Busse F H and Hood L 1978 in preparation
Busse F H and Whitehead J A 1971 *J. Fluid Mech.* **47** 305–20
—— 1974 *J. Fluid Mech.* **66** 67–79
Carroll J J 1971 *The Structure of Turbulent Convection* (*PhD Dissertation* Department of Meteorology, University of California, Los Angeles)
Chan S-K 1971 *Studies Appl. Math.* **50** 13–49
Chandrasekhar S 1961 *Hydrodynamic and Hydromagnetic Stability* (Oxford: Clarendon)
Chang Y P 1957 *Trans. Am. Soc. Mech. Engrs* **79** 1501–13
Chen M M and Whitehead J A 1968 *J. Fluid Mech.* **31** 1–15
Chorin A J 1967 *J. Comp. Phys.* **2** 12–26
Chu T Y and Goldstein R J 1973 *J. Fluid Mech.* **60** 141–50
Clever R M and Busse F H 1974 *J. Fluid Mech.* **65** 625–45
—— 1978 *J. Appl. Math. Phys.* **29**
Davis S H and Segel L A 1968 *Phys. Fluids* **11** 470–6
Deardorff J W 1964 *J. Atmos. Sci.* **21** 419–38
—— 1965 *Phys. Fluids* **8** 1027–30
Dubois M and Berge P 1978 *J. Fluid Mech.* **85** 641–53
Fitzjarrald D E 1976 *J. Fluid Mech.* **73** 693–719
Fromm J E 1965 *Phys. Fluids* **8** 1757–69
Gershuni G Z and Zhukovitskii E M 1976 *Convective Stability of Incompressible Fluids* (Engl. trans. by D Louvish (Jerusalem: Keter Publications))
Gilman P A 1977 *Geophys. Astrophys. Fluid Dyn.* **8** 93–136
Goldstein R J and Chu T Y 1971 *Prog. Heat Mass Transfer* **2** 55–75
Gollup J P, Hulbert S L, Dolny G M and Swinney H L 1977 *Photon Correlation Spectroscopy and Velocimetry* ed H F Cummins and E R Pike (New York: Plenum) pp425–39
Gorkov L P 1957 *Sov. Phys.–JETP* **6** 311–5
Gough D 1977 *Problems of Stellar Convection* ed E A Spiegel and J P Fahn *Springer Lecture Notes in Physics* **71** 15–56
Gough D D, Spiegel E A and Toomre J 1975 *J. Fluid Mech.* **68** 695–719
Graham A 1933 *Phil. Trans. R. Soc.* A **232** 285–96
Gray D D and Giorgini A 1976 *Int. J. Heat Mass Transfer* **19** 545–51
Herring J R 1963 *J. Atmos. Sci.* **20** 325–38
—— 1964 *J. Atmos. Sci.* **21** 277–90
Howard L N 1963 *J. Fluid Mech.* **17** 405–32
—— 1965 *Woods Hole Oceanographic Inst. GFO Notes* No 65–51, I, pp124–6
—— 1966 *Proc. 11th Int. Congr. of Applied Mechanics, Munich, 1964*, ed H Görtler (Berlin: Springer-Verlag) pp1109–15
Jones C A, Moore D R and Weiss N O 1976 *J. Fluid Mech.* **73** 353
Joseph D D 1976 *Stability of Fluid Motions* **2** (Berlin: Springer-Verlag)
Kirchgässner K 1977 *Application of Bifurcation Theory* ed P H Rabinowitz (New York: Academic) pp149–74
Koschmieder E L 1966 *Beitr. Phys. Atmos.* **39** 1–11
—— 1974 *Adv. Chem. Phys.* **26** 177–212
Kraichnan R H 1962 *Phys. Fluids* **5** 1374–89
Krishnamurti R 1968 *J. Fluid Mech.* **33** 457–63
—— 1970a *J. Fluid Mech.* **42** 295–307
—— 1970b *J. Fluid Mech.* **42** 309–20
—— 1973 *J. Fluid Mech.* **60** 285–303
Kuo H L 1961 *J. Fluid Mech.* **10** 611–34

Küppers G 1970 *Phys. Lett.* **32A** 7–8
Küppers G and Lortz D 1969 *J. Fluid Mech.* **35** 609–20
Lipps F B 1976 *J. Fluid Mech.* **75** 113–48
McLaughlin J B and Martin P C 1975 *Phys. Rev.* A **12** 186–203
Malkus W V R 1954a *Proc. R. Soc.* A **225** 185–95
—— 1954b *Proc. R. Soc.* A **225** 196–212
Malkus W V R and Veronis G 1958 *J. Fluid Mech.* **4** 225–60
Mihaljan J M 1962 *Astrophys. J.* **136** 1126–33
Moore D R and Weiss N O 1973 *J. Fluid Mech.* **58** 289–312
Normand C, Pomeau Y and Velarde M G 1977 *Rev. Mod. Phys.* **49** 581–624
Oberbeck A 1879 *Annalen der Physik und Chemie* **7** 271
Palm E 1960 *J. Fluid Mech.* **8** 183–92
—— 1972 *Int. J. Heat Mass Transfer* **15** 2409–17
—— 1975 *Ann. Rev. Fluid Mech.* **7** 39–61
Pellew A and Southwell R V 1940 *Proc. R. Soc.* A **176** 312–43
Plows W H 1971 *Numerical Studies of Laminar, Free Convection in a Horizontal Fluid Layer Heated from Below* (*PhD Thesis* University of California, Berkeley)
Priestley C H B 1954 *Aust. J. Phys.* **7** 176
Proctor M R E 1977 *J. Fluid Mech.* **82** 97–114
Rayleigh (Lord) 1916 *Phil. Mag.* **32** 529–46
Reid W H and Harris D L 1958 *Phys. Fluids* **1** 102–10
Reiss E L 1977 *Application of Bifurcation Theory* ed P H Rabinowitz (New York: Academic) pp37–71
Roberts G O 1978 *Geophys. Astrophys. Fluid Dyn.* in press
Roberts P H 1966 *Non-Equilibrium Thermodynamics, Variational Techniques, and Stability* ed R Donnelly *et al* (Chicago: University of Chicago Press) pp125–62
Robinson J L 1969 *Int. J. Heat Mass Transfer* **12** 1257–65
Rossby H T 1969 *J. Fluid Mech.* **36** 309–35
Ruelle D and Takens F 1971 *Commun. Math. Phys.* **20** 167
Schlüter A, Lortz D and Busse F H 1965 *J. Fluid Mech.* **23** 129–44
Schmidt R J and Saunders O A 1938 *Proc. R. Soc.* A **165** 216–28
Schneck P and Veronis G 1967 *Phys. Fluids* **10** 927–30
Segel L A and Stuart J T 1962 *J. Fluid Mech.* **13** 289–306
Silveston P L 1958 *Forsch. Ing. Wes.* **24** 29–32, 59–69
Somerscales E F C and Dougherty T S 1970 *J. Fluid Mech.* **42** 755–68
Somerscales E F C and Parsapour H 1976 *Bull. Am. Phys. Soc.* **21** 1236
Somerville R C J 1971 *Geophys. Fluid Dyn.* **2** 247–62
Soward A M 1977 *Geophys. Astrophys. Fluid Dyn.* **9** 19–74
Spiegel E A 1962 *Mecanique de la Turbulence* (Paris: CNRS) pp181–201
—— 1971 *Ann. Rev. Astron. Astrophys.* **9** 323–92
—— 1972 *Ann. Rev. Astron. Astrophys.* **10** 261–304
Spiegel E A and Veronis G 1960 *Astrophys. J.* **131** 442–7
Stewartson K 1966 *Non-Equilibrium Thermodynamics, Variational Techniques and Stability* ed R Donnelly *et al* (Chicago: University of Chicago Press) pp158–62
Straus J M 1972 *J. Fluid Mech.* **56** 353–74
—— 1976 *Dyn. Atmos. Oceans* **1** 77–90
Stuart J T 1977 *Application of Bifurcation Theory* ed P H Rabinowitz (New York: Academic)
Threlfall D C 1975 *J. Fluid Mech.* **67** 17–28
Tippelskirch H 1956 *Beitr. Phys. Atmos.* **29** 37–54
Toomre J, Gough D O and Spiegel E A 1977 *J. Fluid Mech.* **79** 1–31
Turner J S 1973 *Buoyancy Effects in Fluids* (Cambridge: Cambridge University Press)
Veronis G 1959 *J. Fluid Mech.* **5** 401–35
—— 1966 *J. Fluid Mech.* **26** 49
—— 1968 *J. Fluid Mech.* **31** 113–39
Wesseling P 1969 *J. Fluid Mech.* **36** 625–37
Whitehead J A and Parsons B 1978 *Geophys. Astrophys. Fluid Dyn.* **9** 201–17
Willis G E and Deardorff J W 1967 *Phys. Fluids* **10** 1861–6
—— 1970 *J. Fluid Mech.* **44** 661–72
Willis G E, Deardorff J W and Somerville R C 1972 *J. Fluid Mech.* **54** 351–67